

# Back-stepping Recursive Decentralized Finite-time Trajectory Tracking Control for Space Parallel Robots with a Bricard Mechanism

Chuandong Guo, Fei Liu, Quan Hu

**Abstract**—A space parallel robot with a Bricard mechanism (SPRBM) is a mechanism for space debris removal. In contrast to traditional serial manipulators, the SPRBM can capture targets of arbitrary shapes, provided the target's envelope falls within the capture range of the SPRBM's net port, with no stringent requirements on the capture point's location. Additionally, owing to the properties of parallel mechanisms, the SPRBM can capture targets possessing greater motion energy than traditional serial manipulators. However, the SPRBM has complicated dynamics, posing significant challenges for dynamic modeling and trajectory tracking control. In this study, we introduce a back-stepping recursive decentralized finite-time control scheme for the trajectory tracking control of the SPRBM. First, the equation of motion for the SPRBM was derived using a recursive algorithm. Then, the back-stepping recursive decentralized finite-time control was formulated, assuming that communication between the decentralized controllers was feasible. The communicated information comprised the relative motion states at the joints, the geometry and mass parameters, and the control torques. Finally, numerical experiments were conducted to validate the effectiveness of the proposed control scheme.

**Index Terms**—Space Parallel Robots; Bricard Mechanism; Recursive Decentralized Control; Back-stepping Finite-time Control.

## I. INTRODUCTION

WITH the development of the aerospace industry, the number of orbital spacecrafts has been continuously increasing. It leads to a large amount of space debris, such as failed satellites and rocket upper stages. The space debris greatly impacts the space environment, seriously threatens the safety of on-orbit spacecrafts, and restricts the sustainable utilization of space resources. Research by NASA [1], [2] has indicated that the preventing the generation of space debris alone is no longer sufficient for the sustainable utilization of space environment; so that, space debris removal has become one of the key issues in the aerospace field. Currently, a variety of removal methods has been developed, such as the flexible tethered capture methods based on flying nets [3]–[6] and harpoons [7] and the rigid capture method using a space robotic arm [8]–[11]. The flexible methods do not have specific requirements for the size and shape of the target to be captured but cannot

This work is supported by the National Natural Science Foundation of China (12272039 and 11972077) and Nature Science Foundation of Sichuan University of Science and Engineering(2024RC03). The authors would like to thank the anonymous reviewers for the valuable comments and suggestions to improve the paper.

Chuandong Guo is with School of Automation and Information Engineering, Sichuan University of Science and Engineering, Yibin, 644005, China and Artificial Intelligence Key Laboratory of Sichuan Province, Yibin, 644005, China. (Email: guochuandong@suse.edu.cn)

Fei Liu is with Beijing Institute of Aerospace Systems Engineering, Beijing, 100076, China. (Email: liufei2775@163.com)

Quan Hu is with Beijing Institute of Technology, Beijing, 100081, China. (Corresponding Author, Email: huquan@bit.edu.cn)

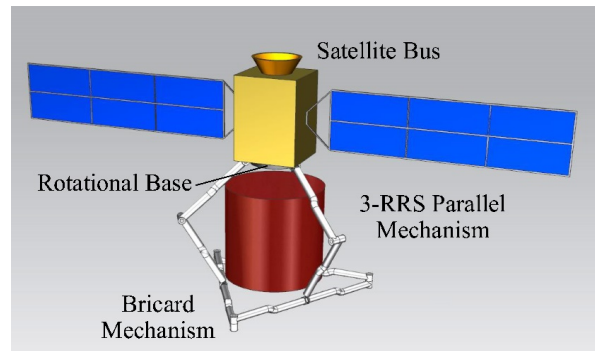


Fig. 1: The space parallel robot (PSR) for on-orbit target capturing [19].

accurately control the target and have limited manipulability. In contrast, the rigid capture method based on space robots has the advantages of high accuracy, controlled capture, and inversible operation (the target can be safely released). The key to this method is the capture points should be carefully chosen and be precisely captured [12]. Space debris is a typical noncooperative object that has different sizes and shapes and with no universal standard interface, making it difficult to determine the appropriate capture points. Moreover, space debris is usually in a rotational state, and thus the capture could pose a great threat for traditional series manipulators. The debris capture system may be out of control or even damaged if the system bearing capacity is insufficient [13].

Compared to traditional series manipulators, parallel robots, such as the space parallel robot with a Bricard mechanism (SPRBM, Fig. 1) proposed by Yao et al. [14], have a better performance in space debris capture tasks. Specifically, SPRBM uses a closed-loop mechanism formed by multiple links to make contacts with the target, and thus, there is no strict requirements for the size of the target, and the mechanism has strong adaptability. The SPRBM is also able to achieve rapid and efficient capture even when the attitude is not in an appropriate initial state [15]. In addition, since the SPRBM adopts a parallel mechanism, it has a high load bearing capacity and, hence, has a better controllability and safety during capture tasks [16]. However, most of the existing studies on the dynamics and control of space-capturing robots focus on the serial mechanism. The SPRBM is a classical multibody system with multi-closed chain constraints, and the dynamics and control problems of the system are very challenging. Current studies on similar mechanisms focus on the kinematic analysis and motion planning [17]–[21]. Therefore, in this work, we investigate the dynamic modeling and trajectory tracking control of a SPRBM.

For the trajectory tracking problem, the existing space robot control schemes can be roughly divided into three categories: centralized control strategies, decentralized control schemes, and recursive decentralized control schemes. Specifically, the centralized control scheme is generally based on the coupling dynamics model of space robots, and the control law is designed while taking the entire system as a whole. The control commands for all joints are solved by the same control

module. Based on the centralized control scheme, a variety of control methods have been proposed to achieve the desired movement of space robots. Jia and Shan [21] studied the finite-time trajectory tracking of a space manipulator in the presence of actuator uncertainties, such as actuator fault, actuator saturation, and bias control torque, and proposed a continuous integral sliding mode controller. By considering the base attitude disturbance, external disturbance, and input constraints, Jin et al. [22] developed an offline model predictive control strategy based on the linear parameter-varying model for free-floating space robots. Shi et al. [23] proposed an optimal adaptive variable structure control method. Taking the motion error as the objective function, the method optimized the control gain using the modified Gaussian barebones differential evolution method, to deal with uncertainty and external disturbance in real time. For a six-degree of freedom (DOF) rigid space manipulator subject to an inaccurate dynamic model, Fan and Jing [24] designed a trajectory tracking controller with specified time convergence based on the appointed-time reachable performance function. The above control methods are effective to deal with system dynamics uncertainty, actuator uncertainty, and disturbances and have high control accuracy. However, such centralized control schemes require real-time calculation of robot dynamics model and nonlinear terms, resulting in a computation volume and memory usage.

To reduce the calculations burden on the controllers' hardware, the decentralized control scheme was developed. In the decentralized control, each link is regarded as a subsystem of the robot, and the coupling terms between subsystems are considered as disturbances. Therefore, the decentralized control scheme does not need to compensate for the coupled interactions inside the robot, which reduces the dependence on the system model, thus, the calculation volume and memory usage. However, one disadvantage of the decentralized control scheme is the control accuracy of the system would be reduced since all the coupling are viewed as disturbances. Common decentralized control schemes include decentralized proportional-derivative (PD) controllers [25], as well as many decentralized robust controllers. Tang et al. [26] proposed a decentralized controller for mechanical systems based on the boundedness of the high-order interconnections. For modular robot manipulators, Dong et al. [27] developed a decentralized robust optimal controller based on the critic-identifier structure-based adaptive dynamic programming scheme. In the controller, neural network identifiers were used to estimate the coupling factors between subsystems. Considering the influence of environmental uncertainties, Dong et al. [28] designed a decentralized robust zero-sum optimal control approach based on the adaptive dynamic programming algorithm. For the above decentralized control scheme, the authors either did not consider the interaction between subsystems or did not estimate the coupling of subsystems using identifiers; thus, the control accuracy of such schemes remains relatively low.

In essence, the multibody robotic system is composed of interrelated subsystems. On this basis, the multibody system dynamics model based on the recursive algorithm was proposed [29]. Based on the multibody characteristic, Hu et al. [30] proposed a recursive decentralized control scheme.

Shen et al. [31] designed a recursive decentralized finite-time controller. Su et al. [32] applied recursive decentralized control to flexible space manipulators and designed the recursive decentralized adaptive robust controller for trajectory tracking and vibration suppression of a flexible space manipulator. In summary, the recursive decentralized control combines the recursive multibody system with the decentralized control scheme, thereby achieving a balance between centralized control and decentralized control schemes. Compared to standard centralized control schemes, the recursive decentralized control scheme does not require accurate centralized dynamics models, thereby reducing the amount of calculation. Compared to the decentralized control scheme, the recursive decentralized control scheme fully utilizes the interaction between subsystems, thereby improving the control performance.

However, to get a recursive decentralized controller of the SPRBM, two issues must be addressed at first. One is how to establish the recursive dynamics model of the SPRBM which is suitable for a recursive decentralized control scheme. Due to the complex structure with 4 closed-loop mechanisms of the SPRBM, how to overcome the closed-loop constraints to obtain the recursive dynamics model which can be directly used in the design of the control scheme is the primary challenge. The second challenge is how to design an effective controller to ensure the stability of the SPRBM with complex dynamic forms.

In the present study, for the novel mechanism SPRBM, a recursive dynamics model is firstly developed. Then, a single-input and single-output controller is designed for each independent joint, and the influence of the state of adjacent links on the motion of each joint is considered in the control law. Theoretically, a recursive decentralized control scheme can achieve better real-time performance and lower memory usage than centralized control and higher control accuracy than decentralized control. To design the control law, back-stepping [33], [34] and finite-time control [35]–[37] are combined, which can not only ensure the stability of the closed-loop system but also increase the robustness of the system and ensure the finite-time convergence of the system [38]–[40].

Compared with current studies on SPRBM and similar mechanisms focusing on kinematic analysis and motion planning, the main innovation of the present work is twofold. On one side, the recursive dynamics model for the SPRBM is established. Since the SPRBM is a multibody system with complex configuration, its recursive dynamics model will facilitate the required modeling and simulation. On the other side, a back-stepping recursive decentralized finite-time control is formulated based on the model in the recursive form. The obtained controller has high computational efficiency since the control input is calculated recursively, and with enough control accuracy due to the incorporation of the system dynamics.

The structure of the manuscript is as follows: Section II presents the structure of the SPRBM, as well as the definition of the generalized coordinates of the system. The installation positions of the driving motor and the sensors were configured. The recursive dynamics model of the SPRBM is given in Section III. The back-stepping recursive decentralized finite-time controller is developed in Section IV. Then, Section V

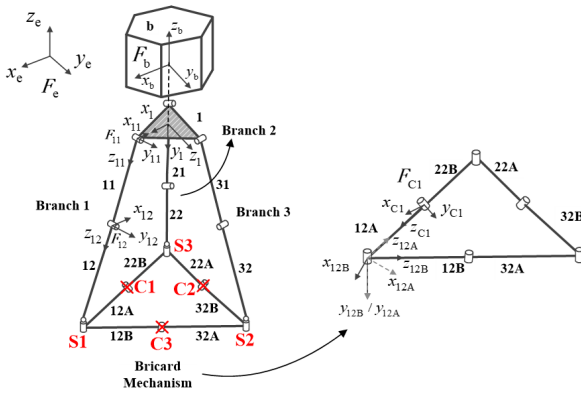


Fig. 2: Sketch of the SPRBM and Bricard mechanism [19].

illustrates the effectiveness of the proposed SPRBM controller using numerical simulations. Conclusions are drawn in Section VI.

## II. SYSTEM DESCRIPTION OF THE SPRBM

### A. System Description

As shown in Fig. 1, the SPRBM is composed of four components: satellite bus, rotational base, a 3RRS (revolute-revolute-spherical joint) parallel mechanism, and a Bricard mechanism. The satellite bus and the rotational base are named Link b and Link 1, respectively, which are connected by a revolute joint. Each branch of the 3RRS parallel mechanism is composed of two revolute joints and one spherical joint, while the links are numbered by the branch they belong to (i.e., 11, 12, 21, 22, 31, and 32). The Bricard mechanism consists of six links, which are named 12A, 12B, 22A, 22B, 32A, and 32B, as shown in Fig. 2. The links are connected by revolute joints. The angle between two adjacent revolute joints is limited within  $\pm 30^\circ$ . The numbering of the revolute joints of the 3RRS parallel mechanism is consistent with that of the outboard links. The spherical joints and the revolute joints in the Bricard mechanism are named S1 S3 and C1 C3, respectively. The inertial frame  $F_e$  and body-fixed frames of each link are also defined in Fig. 2.

### B. Generalized Coordinates

Fig. 2 shows that there are three closed-loop mechanisms between the 3RRS parallel mechanism and the Bricard mechanism. The closed-loop constraints of joints C1-C3 are eliminated, and two new end bodies are generated, numbered A and B, respectively. Hence, the constraints of the three revolute joints are removed, that is, 15 constraint equations. The topology of the unconstrained system is shown in Fig. 3. The system has a total of 25 degrees of freedom, and thus, a total of 25 generalized velocities are needed to describe the system state. The generalized speeds are chosen as

$$\mathbf{q} = [\mathbf{q}_b^T, \dot{\mathbf{q}}_\theta^T]^T \in \mathbb{R}^{25 \times 1} \quad (1)$$

where  $\mathbf{q}_b = [\mathbf{v}_b^T, \omega_b^T]^T \in \mathbb{R}^{6 \times 1}$ ,  $\mathbf{v}_b$  and  $\omega_b$  are the inertial velocity and angular velocity of  $F_b$  relative to  $F_e$ , respectively.  $\dot{\mathbf{q}}_\theta$  is the relative angular velocity in each joint, which can be

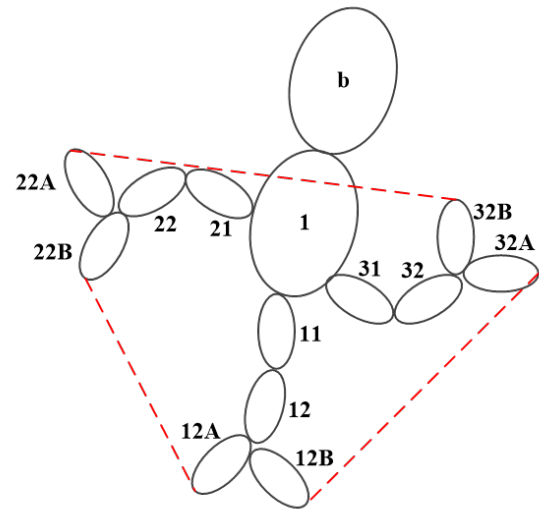


Fig. 3: Topology of the unconstrained system [19].

defined by the motion of each body-fixed frame relative to its inboard body-fixed frame and can be written as

$$\dot{\mathbf{q}}_\theta = [\dot{\theta}_1, \dot{\theta}_{11}, \dot{\theta}_{21}, \dot{\theta}_{31}, \dot{\theta}_{12}, \dot{\theta}_{22}, \dot{\theta}_{32}, \omega_{12A}^T, \omega_{22A}^T, \omega_{32A}^T, \dot{\theta}_{12B}, \dot{\theta}_{12B}, \dot{\theta}_{22B}, \dot{\theta}_{32B}]^T \in \mathbb{R}^{19 \times 1} \quad (2)$$

According to Ref. [19] considering the configuration singularities and reliability of the SPRBM, the driving motors are allocated in joints #1, #11, #21, #31 and in joints C1 C3. Then, the independent generalized speeds of the SPRBM are chosen as

$$\mathbf{q}_I = [\mathbf{v}_b^T, \omega_b^T, \dot{\theta}_1, \dot{\theta}_{11}, \dot{\theta}_{21}, \dot{\theta}_{31}, \dot{\theta}_{12B}]^T \in \mathbb{R}^{11 \times 1} \quad (3)$$

whereas the dependent generalized speeds are

$$\mathbf{q}_D = [\dot{\theta}_{12}, \dot{\theta}_{22}, \dot{\theta}_{32}, \omega_{12A}^T, \omega_{22A}^T, \omega_{32A}^T, \dot{\theta}_{22B}, \dot{\theta}_{32B}]^T \in \mathbb{R}^{14 \times 1} \quad (4)$$

It is worth noting that the driving motors are redundantly configured at this point. The relationship between the independent joint control variable  $\mathbf{u}_I \in \mathbb{R}^{5 \times 1}$  and the driving joint control variable  $\mathbf{u}_M \in \mathbb{R}^{7 \times 1}$  can be described by the following constraint equation

$$\mathbf{G}_{IM}\mathbf{u}_M = \mathbf{u}_I \quad (5)$$

where  $\mathbf{G}_{IM} \in \mathbb{R}^{5 \times 7}$  is the constraint matrix. Eq.(5) is an underdetermined linear equation, and the minimum two-norm solution  $\mathbf{u}_{Mp} = \mathbf{G}_{IM}^+ \mathbf{u}_I$  can be obtained via the pseudoinverse operation. Since the driving motors in the Bricard mechanism are symmetrical, the objective of the pseudoinverse method is to distribute  $\mathbf{u}_I$  evenly among the three motors such that the sum of the squares of the absolute values of the output torques is minimal. In the case of one or two driving motor failures in the Bricard mechanism,  $\mathbf{u}_I$  can still be distributed evenly to active driving motors using the above method.

TABLE I: Quality and Dimension Parameters of SPRBM [19].

Quality Parameters		Dimension Parameters	
Mass of the satellite bus $m_b/\text{kg}$	12.5	Length of the satellite bus $a_b/m$	0.3
Inertia of the satellite bus $\mathbf{J}_{Cb}/\text{kg} \cdot \text{m}^2$	diag(1.2, 1.2, 0.8)	Height of the satellite bus $h_b/m$	0.5
Mass of the rotational base $m_1/\text{kg}$	1.2	Radius of the rotational base $r_1/m$	0.1
Inertia of the rotational base $\mathbf{J}_{C1}/\text{kg} \cdot \text{m}^2$	diag(0.025, 0.045, 0.025)	Height of the rotational base $h_1/m$	0.08
Mass of other links $m_i/\text{kg}$	0.6	Length of other links $l/m$	0.5
Inertia of other links $\mathbf{J}_{Ci}/\text{kg} \cdot \text{m}^2$	diag(0.017, 0.017, 0.0003)	Height of other links $r_L/m$	0.02

As for the configuration of the sensors, due to the requirements of the controller, motion sensors for joint rotation angle and angular velocity measurements are installed at the joints where the driving motors are located. The motion of other joints is calculated based on the measurement data and the kinematics relationship between joints. The SPRBM may come into contact with the target at multiple points. If the contact force is directly measured by force sensors placed on the surface of each link, the system reliability will be greatly reduced. Thus, we can only measure the generalized active force due to external contact at each joint. On the one hand, the robot has multiple closed-loop mechanisms, and the internal constraint force or constraint torque of each closed-loop mechanism could be measured using force sensors, thereby facilitating the calculation of the generalized force introduced by the external contact. On the other hand, since the Bricard mechanism has redundant constraints, from a theoretical point of view, the internal constraint force of each joint may have an infinite number of solutions. In actual conditions, the joint force is related to the installation error and deformations in the system. Therefore, to accurately obtain the constraint force of each joint and to achieve high-precision control, taking the system symmetry and its mechanical structure into consideration, six-dimensional force/torque sensors are installed at the three driving joints of the Bricard mechanism.

### III. EQUATION OF MOTION OF THE SPRBM

Without considering the flexibility of the joints and links, the SPRBM is regarded as a rigid multibody body system. In this section, the recursive relationship between the kinematics and dynamics of two adjacent rigid bodies is established based on the method in Hu et al. [29], thereby obtaining the recursive dynamics model of the rigid multibody body system. The spatial vector algebra used in this section is shown in Appendix A in detail.

#### A. Recursive Kinematics

Fig. 4 shows an arbitrary Link  $j$ . Its inboard and outboard body-fixed frames are denoted as  $c(j)$  and  $o(j)$ , respectively. The joint  $h_j$  between  $j$  and  $c(j)$  connects point  $O_j$  and point  $O_{c(j)}^{h_j}$  on the two links. The origin of the body-fixed frame  $F_j$  is  $O_j$ , which is fixed to Link  $j$ . The origin of the coordinate frame  $F_{Qj}$  is  $O_{c(j)}^{h_j}$ , which is fixed to Link  $c(j)$ .

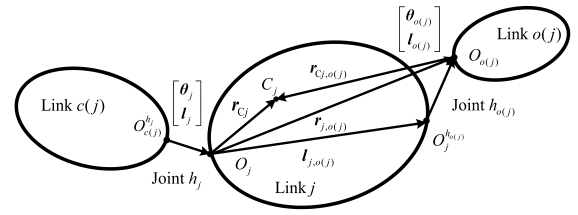


Fig. 4: A serial mechanism consisting of a link and two adjacent links.

The rotation angle of the joint  $h_{o(j)}$  is defined as  $\theta_{o(j)}$  within the  $F_{o(j)}$  of Link  $o(j)$ . The coordinate transformation matrix from  $F_{o(j)}$  to  $F_j$  is denoted as  $\mathbf{A}_{j,o(j)}$ , which can be calculated based on the relative rotation between  $F_j$  and  $F_{Qo(j)}$  and the rotation  $\theta_{o(j)}$  between  $o(j)$  and  $j$ .

In  $F_j$ , the following position vectors are defined:  $\mathbf{r}_{j,o(j)}$  is the position of point  $O_{o(j)}$  relative to point  $O_j$ .  $\mathbf{r}_{Cj}$  and  $\mathbf{r}_{Cj,o(j)}$  denote the position of the centroid  $C_j$  relative to point  $O_j$  and point  $O_{c(j)}$ .  $\mathbf{l}_{j,o(j)}$  is the position of point  $O_j^{h_{o(j)}}$  relative to point  $O_j$ . In  $F_{o(j)}$ ,  $\mathbf{l}_{o(j)}$  is the displacement of joint  $h_{o(j)}$  in the direction of the degree of freedom. Then, the vector  $\mathbf{r}_{j,o(j)}$  can be calculated from  $\mathbf{l}_{j,o(j)}$  and  $\mathbf{l}_{o(j)}$ .  $\mathbf{r}_{Cj}$ , and  $\mathbf{r}_{Cj,o(j)}$  satisfy the following relationship

$$\mathbf{r}_{j,o(j)} + \mathbf{r}_{Cj,o(j)} = \mathbf{r}_{Cj} \quad (6)$$

If Link  $j$  has multiple outboard body-fixed frames,  $o(j_m)$  ( $m = 1, 2, \dots, M$ ), then, Links  $j$  and  $o(j_m)$  can be described in the same manner given above.

According to the theory of multibody dynamics, the absolute velocity of Link  $j$  in the inertial space is a linear combination of the generalized speeds:

$$\mathbf{V}_j = \mathbf{J}_{Vj} \boldsymbol{\Gamma}_T \mathbf{q} \quad (7)$$

where  $\boldsymbol{\Gamma}_T$  is the block diagonal matrix constituted by the projection matrix  $\boldsymbol{\Gamma}_{Ti}$  ( $i = 1, 2, \dots, n$ ),  $\mathbf{q}$  is the generalized speeds column matrix constituted by  $\mathbf{q}_i$  ( $i = 1, 2, \dots, n$ ), and  $n$  is the number of rigid bodies in the system. Consider two adjacent rigid bodies  $c(j)$  and  $j$ , there is a recursive

relationship between the absolute velocities of the two:

$$\dot{\mathbf{V}}_j = \bar{\mathbf{A}}_{c(j),j}^T \tilde{\mathbf{r}}_{c(j),j}^T \mathbf{V}_{c(j)} + \Gamma_{Tj} \dot{\mathbf{q}}_j \quad (8)$$

where  $\bar{\mathbf{A}}_{c(j),j}^T$  is defined in the same manner in Eq. (51). The coupled kinematics model in Eq. (7) is essentially equivalent to the recursive kinematics model in Eq. (8). This is because Eq. (8) holds true for any body and its inboard body-fixed frame in the system. By sequentially substituting the recursive kinematics of each inboard body-fixed frame of Link  $j$  into Eq. (8), the kinematics model in Eq. (7) will be obtained, and

$$\mathbf{J}_{Vj} = \left[ \bar{\mathbf{A}}_{1,j}^T \tilde{\mathbf{r}}_{1,j}^T, \dots, \bar{\mathbf{A}}_{c(j),j}^T \tilde{\mathbf{r}}_{c(j),j}^T, \mathbf{U}, \mathbf{0}, \dots, \mathbf{0} \right] \quad (9)$$

By taking the derivative of Eqs. (7) and (8), we have

$$\begin{aligned} \dot{\mathbf{V}}_j &= \mathbf{J}_{Vj} \Gamma_T \dot{\mathbf{q}} + \dot{\mathbf{J}}_{Vj} \Gamma_T \mathbf{q} \\ &= \bar{\mathbf{A}}_{c(j),j}^T \tilde{\mathbf{r}}_{c(j),j}^T \dot{\mathbf{V}}_{c(j)} + \left( \bar{\mathbf{A}}_{c(j),j}^T \tilde{\mathbf{r}}_{c(j),j}^T \right)' \mathbf{V}_{c(j)} + \Gamma_{Tj} \dot{\mathbf{q}}_j \end{aligned} \quad (10)$$

$\dot{\mathbf{V}}_j$  is divided into a linear part  $\dot{\mathbf{V}}_{j0} = \mathbf{J}_{Vj} \Gamma_T \dot{\mathbf{q}}$  and a nonlinear part  $\dot{\mathbf{V}}_{jt} = \dot{\mathbf{J}}_{Vj} \Gamma_T \mathbf{q}$ . Similarly,  $\dot{\mathbf{V}}_{c(j)}$  is also divided into a linear part  $\dot{\mathbf{V}}_{c(j)0}$  and a nonlinear  $\dot{\mathbf{V}}_{c(j)t}$ . Then, Eq. (7) can be written as

$$\begin{aligned} \dot{\mathbf{V}}_j &= \dot{\mathbf{V}}_{j0} + \dot{\mathbf{V}}_{jt} \\ &= \bar{\mathbf{A}}_{c(j),j}^T \tilde{\mathbf{r}}_{c(j),j}^T \dot{\mathbf{V}}_{c(j)0} + \Gamma_{Tj} \dot{\mathbf{q}}_j + \bar{\mathbf{A}}_{c(j),j}^T \tilde{\mathbf{r}}_{c(j),j}^T \dot{\mathbf{V}}_{c(j)t} \\ &\quad + \left( \bar{\mathbf{A}}_{c(j),j}^T \tilde{\mathbf{r}}_{c(j),j}^T \right)' \mathbf{V}_{c(j)} \end{aligned} \quad (11)$$

Thus the recursive relation of the linear part  $\dot{\mathbf{V}}_{j0}$  is taken as the recursive kinematics equation between  $c(j)$  and  $j$ . Then,

$$\dot{\mathbf{V}}_{j0} = \bar{\mathbf{A}}_{c(j),j}^T \tilde{\mathbf{r}}_{c(j),j}^T \dot{\mathbf{V}}_{c(j)0} + \Gamma_{Tj} \dot{\mathbf{q}}_j \quad (12)$$

It is worth noting that the nonlinear part  $\dot{\mathbf{V}}_{jt}$  satisfies the following recursive relation,

$$\dot{\mathbf{V}}_{jt} = \bar{\mathbf{A}}_{c(j),j}^T \tilde{\mathbf{r}}_{c(j),j}^T \dot{\mathbf{V}}_{c(j)t} + \left( \bar{\mathbf{A}}_{c(j),j}^T \tilde{\mathbf{r}}_{c(j),j}^T \right)' \mathbf{V}_{c(j)} \quad (13)$$

### B. Recursive Dynamics

The equations of motion of a multibody system can be written in a coupled manner,

$$\mathbf{M} \ddot{\mathbf{q}} = \mathbf{F}_A - \mathbf{F}_t \quad (14)$$

where  $\mathbf{M}$  is the system mass matrix, and  $\mathbf{F}_A = [\mathbf{F}_{A1}^T, \mathbf{F}_{A2}^T, \dots, \mathbf{F}_{An}^T]^T$  and  $\mathbf{F}_t = [\mathbf{F}_{t1}^T, \mathbf{F}_{t2}^T, \dots, \mathbf{F}_{tn}^T]^T$  are the nonlinear terms of the generalized active force and the generalized inertial force corresponding to each generalized velocity, respectively. However, we will rewrite the dynamics

in a recursive form, so that the controller can be designed in a model with lower dimension.

Consider two adjacent rigid bodies  $j$  and  $o(j)$ , when Link  $j$  has only one outboard body-fixed frame, the dynamic equation of the rigid body  $j$  can be written as follows using the kinematics relation in Eq. (11),

$$\mathbf{I}_j \left( \dot{\mathbf{V}}_{j0} + \dot{\mathbf{V}}_{jt} \right) + \mathbf{X}_j = \mathbf{F}_{Hj} - \tilde{\mathbf{r}}_{j,o(j)} \bar{\mathbf{A}}_{j,o(j)} \mathbf{F}_{Ho(j)} \quad (15)$$

where  $\mathbf{I}_j$  is given in Eq. (56); the wrench  $\mathbf{F}_{Hj}$  and  $\mathbf{F}_{Ho(j)}$  are the sum of the active force and the constraint force/torque between Link  $j$  and  $o(j)$  and its inboard body-fixed frame, respectively.  $\mathbf{X}_j$  is the nonlinear term of the generalized inertial force in the single rigid body dynamic equation in the inertial space.

If the constraint forces/torques between the bodies are measurable, the above equations can be combined with the recursive kinematics equation and used as a recursive decentralized controller model. Because only the closed-loop constraints on C1-C3 are removed and force sensors are installed on C1-C3, the constraint forces/torques are only measurable at those locations. Therefore, the joint motion information should be used to replace the constraint forces/torques in the above equation.

Based on Eq. (15), when Link  $o(j)$  is an end body formed after removing a closed-loop constraint, its dynamics equation is written as

$$\mathbf{I}_{1o(j)} \dot{\mathbf{V}}_{o(j)0} = \mathbf{F}_{Ho(j)} - \mathbf{F}_{TXo(j)} \quad (16)$$

where

$$\begin{cases} \mathbf{I}_{1o(j)} = \mathbf{I}_{o(j)} \\ \mathbf{F}_{TXo(j)} = \mathbf{X}_{o(j)} + \mathbf{I}_{o(j)} \dot{\mathbf{V}}_{o(j)t} + \tilde{\mathbf{r}}_{o(j),o(j)x}^o \mathbf{F}_{So(j),x} \end{cases} \quad (17)$$

where  $\mathbf{F}_{o(j),x}$  is the constraint force/torque of the closed-loop constraint, which is measured by the force sensor.  $\tilde{\mathbf{r}}_{o(j),o(j)x}^o = \tilde{\mathbf{r}}_{o(j),o(j)x} \bar{\mathbf{A}}_{o(j),o(j)x}$ , and  $\mathbf{r}_{o(j),o(j)x}$  is the position of the point  $O_{o(j)x}$  relative to  $O_{o(j)}$ .

Eq. (16) is left multiplied by  $\Gamma_{To(j)}^T$  and then projected to the generalized velocity space of the link, we have

$$\begin{aligned} \dot{\mathbf{q}}_{o(j)} &= -\mathbf{I}_{qo(j)}^{-1} \Gamma_{To(j)}^T \left( \mathbf{I}_{o(j)} \tilde{\mathbf{r}}_{j,o(j)}^{oT} \dot{\mathbf{V}}_{j0} + \mathbf{F}_{TXo(j)} \right) \\ &\quad + \mathbf{I}_{qo(j)}^{-1} \mathbf{F}_{Ao(j)} \end{aligned} \quad (18)$$

where

$$\mathbf{I}_{qo(j)} = \Gamma_{To(j)}^T \mathbf{I}_{1o(j)} \Gamma_{To(j)} \quad (19)$$

Substituting Eq. (18) into Eq. (16), the joint force is obtained:

$$\begin{aligned} \mathbf{F}_{Ho(j)} &= \mathbf{\Gamma}_{qo(j)} \mathbf{I}_{o(j)} \tilde{\mathbf{r}}_{j,o(j)}^{\circ T} \dot{\mathbf{V}}_{j0} + \mathbf{\Gamma}_{qo(j)} \mathbf{F}_{TXo(j)} \\ &+ \mathbf{I}_{o(j)} \mathbf{\Gamma}_{To(j)} \mathbf{I}_{qo(j)}^{-1} \mathbf{F}_{Ao(j)} \end{aligned} \quad (20)$$

where  $\mathbf{\Gamma}_{qo(j)} = \mathbf{U} - \mathbf{I}_{o(j)} \mathbf{\Gamma}_{To(j)} \mathbf{I}_{qo(j)}^{-1} \mathbf{\Gamma}_{To(j)}^T$ .

Eq. (20) is substituted into the dynamics equation of the inboard body-fixed frame of  $o(j)$  to remove the interbody constraint force

$$\mathbf{I}_{1j} \dot{\mathbf{V}}_{j0} = \mathbf{F}_{Hj} - \mathbf{F}_{TXj} \quad (21)$$

where

$$\left\{ \begin{array}{l} \mathbf{I}_{1j} = \mathbf{I}_j + \tilde{\mathbf{r}}_{j,o(j)}^{\circ T} \mathbf{I}_{o(j)} \mathbf{\Gamma}_{qo(j)} \tilde{\mathbf{r}}_{j,o(j)}^{\circ T} \\ \mathbf{F}_{TXj} = \mathbf{X}_j + \mathbf{I}_j \dot{\mathbf{V}}_{jt} + \tilde{\mathbf{r}}_{j,o(j)}^{\circ T} (\mathbf{\Gamma}_{qo(j)} \mathbf{F}_{TXo(j)} \\ + \mathbf{I}_{o(j)} \mathbf{\Gamma}_{To(j)} \mathbf{I}_{qo(j)}^{-1} \mathbf{F}_{Ao(j)}) \end{array} \right. \quad (22)$$

Eq. (21) is projected to the generalized velocity space:

$$\dot{\mathbf{q}}_j = -\mathbf{I}_{qj}^{-1} \mathbf{\Gamma}_{Tj}^T \left( \mathbf{I}_{1j} \tilde{\mathbf{r}}_{c(j),j}^{\circ T} \dot{\mathbf{V}}_{c(j)0} + \mathbf{F}_{Tx,j} \right) + \mathbf{I}_{qj}^{-1} \mathbf{F}_{Aj} \quad (23)$$

where

$$\mathbf{I}_{qj} = \mathbf{\Gamma}_{Tj}^T \mathbf{I}_{1j} \mathbf{\Gamma}_{Tj} \quad (24)$$

Eqs. (16)-(19) are special forms of Eqs. (21)-(24) when there are no outboard body-fixed frames; hence, the above process can be recursively performed from the system end body to the root body. For a node with  $M$  outboard body-fixed frames, the recursive form of Eq. (22) can be written as

$$\left\{ \begin{array}{l} \mathbf{I}_{1j} = \mathbf{I}_j + \sum_{m=1}^M \tilde{\mathbf{r}}_{j,o(j_m)}^{\circ T} \mathbf{I}_{o(j_m)} \mathbf{\Gamma}_{qo(j_m)} \tilde{\mathbf{r}}_{j,o(j_m)}^{\circ T} \\ \mathbf{F}_{TXj} = \mathbf{I}_j \dot{\mathbf{V}}_{jt} + \sum_{m=1}^M \tilde{\mathbf{r}}_{j,o(j_m)}^{\circ T} (\mathbf{\Gamma}_{qo(j_m)} \mathbf{F}_{TXo(j_m)} \\ + \mathbf{I}_{o(j_m)} \mathbf{\Gamma}_{To(j_m)} \mathbf{I}_{qo(j_m)}^{-1} \mathbf{F}_{Ao(j_m)}) + \mathbf{X}_j \end{array} \right. \quad (25)$$

According to Eqs. (18) and (23), the dynamics equation of Link  $i$  considering the presence of a disturbance is written as

$$\mathbf{I}_{qi0} \dot{\mathbf{q}}_{\theta i} = -\mathbf{\Gamma}_{Ti}^T \mathbf{I}_{1i0} \sum_{k=1}^{c(i)} \tilde{\mathbf{r}}_{k,i}^{\circ T} \mathbf{\Gamma}_{Tk} \dot{\mathbf{q}}_{\theta k} - \mathbf{\Gamma}_{Ti}^T \mathbf{F}_{Tx,i} + \mathbf{u}_i + \mathbf{d}_{xi} \quad (26)$$

where  $\mathbf{I}_{qi0}$  and  $\mathbf{I}_{1i0}$  are the nominal terms corresponding to  $\mathbf{I}_{qi}$  and  $\mathbf{I}_{1i}$ , respectively.  $\mathbf{d}_{xi}$  is the disturbance term caused by mass uncertainty, force sensor measurement error, the joint motion of the manipulator due to satellite movement, and/or other external environmental factors.  $\mathbf{u}_i$  is the control input corresponding to  $\mathbf{F}_{Ai}$ .

### C. Discussions on the equations of motion

The tracking error state variables of each independent joint of the manipulator are denoted as  $\mathbf{x}_1 = \theta_i - \theta_{d,i}$  and  $\mathbf{x}_2 = \mathbf{q}_{\theta i} - \mathbf{q}_{d,\theta i}$ . Where  $\mathbf{x}_1, \mathbf{x}_2 \in \mathbb{R}^{5 \times 1}$ , and  $\theta_{d,i}$  and  $\mathbf{q}_{d,\theta i}$  are the desired rotation angle and angular velocity of the independent joint, respectively. The state variables in the generalized velocity space are  $\mathbf{x}_{\theta 1} = \theta - \theta_d$  and  $\mathbf{x}_{\theta 2} = \mathbf{q}_{\theta} - \mathbf{q}_{d,\theta}$ , where  $\mathbf{x}_{\theta 1}, \mathbf{x}_{\theta 2} \in \mathbb{R}^{19 \times 1}$ , and  $\theta_d$  and  $\mathbf{q}_{d,\theta}$  are the desired rotation angle and angular velocity of each joint, respectively. Due to the presence of closed-loop constraints, the motion of each joint can be determined by the independent generalized velocity, and the above relationship can be written as  $\mathbf{q}_{\theta} = \mathbf{G}_{\theta I} \mathbf{q}_{\theta I}$  and  $\mathbf{q}_{d,\theta} = \mathbf{G}_{d,\theta I} \mathbf{q}_{d,\theta I}$ . Then,

$$\mathbf{x}_{\theta 2} = \mathbf{G}_{\theta I} \mathbf{x}_2 - (\mathbf{G}_{d,\theta I} - \mathbf{G}_{\theta I}) \mathbf{q}_{d,\theta I} \quad (27)$$

It can be proved that when  $\mathbf{x}_1, \mathbf{x}_2 \rightarrow 0$ , we have  $\mathbf{x}_{\theta 1}, \mathbf{x}_{\theta 2} \rightarrow 0$ . Therefore, the recursive decentralized controllers can still be designed in the independent generalized velocity space. Since the independent generalized velocity  $\mathbf{q}_{\theta I}$  is for column hinge joints, according to Eq. (26), the model of the recursive decentralized trajectory tracking controller for the  $i$ th independent joint can be written as

$$\left\{ \begin{array}{l} \dot{\mathbf{x}}_{1,i} = \mathbf{x}_{2,i} \\ \dot{\mathbf{x}}_{2,i} = I_{q0,\theta i}^{-1} (-F_{Tx,\theta i} - \dot{q}_{d,\theta i}^{rd} \\ + d_{x,\theta i}^{rd} + d_{x,\theta i} + u_{\theta i,i}) - \dot{q}_{d,\theta i} \end{array} \right. \quad (i = 1, 2, \dots, 5) \quad (28)$$

where  $F_{Tx,\theta i} = \mathbf{\Gamma}_{T,\theta i}^T \mathbf{F}_{Tx,\theta i}$ ;  $\dot{q}_{d,\theta i}^{rd}$  is the desired generalized acceleration coupling term, and  $\dot{q}_{d,\theta i}^{rd} = \mathbf{\Gamma}_{T,\theta i}^T \mathbf{I}_{10,\theta i} \sum_{k=1}^{c(\theta i)} \tilde{\mathbf{r}}_{k,\theta i}^{\circ T} \mathbf{\Gamma}_{Tk} \dot{\mathbf{q}}_{d,\theta k}$ . Since it is difficult to measure joint acceleration, the influence of the acceleration tracking error of each inboard body-fixed frame on the joint motion is taken as a disturbance,  $d_{\theta,\theta i}^{rd} = -\mathbf{\Gamma}_{T,\theta i}^T \mathbf{I}_{10,\theta i} \sum_{k=1}^{c(\theta i)} \tilde{\mathbf{r}}_{k,\theta i}^{\circ T} \mathbf{\Gamma}_{Tk} \dot{\mathbf{x}}_{\theta 2,k}$ . Here the superscript 'rd' characterizes the influence of the inboard bodies in recursive dynamics.  $d_{x,\theta i}$  is the disturbance caused by force sensor measurement error, joint motion of the manipulator due to satellite movement, and other external environmental factors.  $u_{\theta i,i}$  is the control variable to be designed. The other items can be calculated recursively using Eq. (25). Then, the recursive decentralized controller based on Eq. (28) is shown in Fig. 5.

The disturbances in Eq. (28) include  $d_{x,\theta i}$  and  $d_{\theta,\theta i}^{rd}$ . According to the definition of  $d_{x,\theta i}$ , because the velocity, angular acceleration, and force sensor measurement error are bounded in practical engineering,  $d_{x,\theta i}$  is bounded.  $d_{\theta,\theta i}^{rd}$  is the disturbance of the motion of each inboard body-fixed frame of the  $i$ th independent joint, which is written as the linear combination of the components in  $\dot{\mathbf{x}}_{\theta 2}$ . According to Eq. (27), the system states  $\dot{\mathbf{x}}_{\theta 2}$  and  $\dot{\mathbf{x}}_2$  satisfy the following relation

$$\begin{aligned} \dot{\mathbf{x}}_{\theta 2} &= \mathbf{G}_{\theta I} \dot{\mathbf{x}}_2 + \dot{\mathbf{G}}_{\theta I} \mathbf{x}_2 - (\mathbf{G}_{d,\theta I} - \mathbf{G}_{\theta I}) \dot{q}_{d,\theta I} \\ &- (\dot{\mathbf{G}}_{d,\theta I} - \dot{\mathbf{G}}_{\theta I}) \mathbf{q}_{d,\theta I} \end{aligned} \quad (29)$$

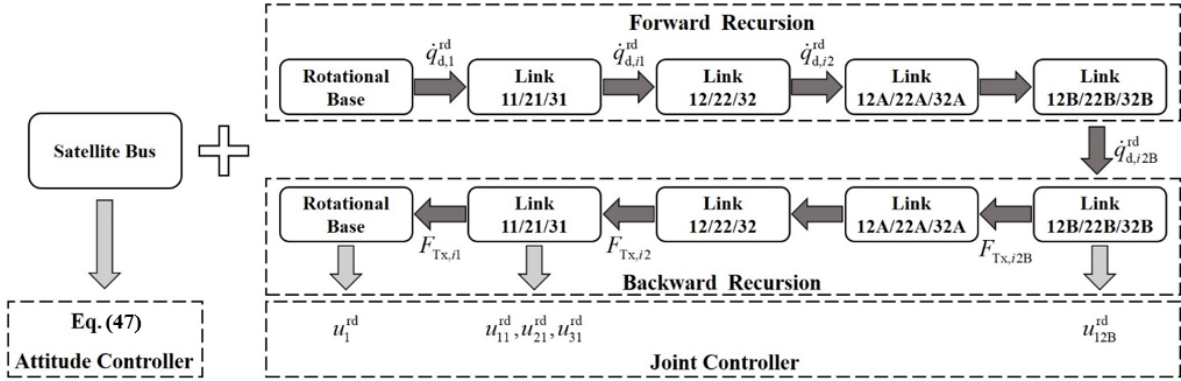


Fig. 5: Architecture of the recursive decentralized controller.

$\dot{\mathbf{x}}_{\theta 2}$  is the sum of the linear combination of  $\dot{\mathbf{x}}_2$ ,  $\mathbf{x}_2$ , and a bounded nonlinear term.  $\dot{\mathbf{x}}_2$  is a bounded function of the state variables  $\mathbf{x}_1$ ,  $\mathbf{x}_2$ , and control variables of the joint that correspond to the independent generalized velocity [26]. Moreover, the mass and structural parameters of the system are known in practical engineering. In summary, the disturbance in Eq. (28) satisfies the following boundary conditions [41]

$$I_{q0,\theta i}^{-1} |d_{\theta,\theta i}^{\text{rd}} + d_{x,\theta i}| \leq \sum_{j=1}^5 \delta_{ij} D_j \quad (30)$$

where  $\delta_{ij} \geq 0$ ,  $D_j = 1 + |x_{1,j}| + |x_{2,j}| + |x_{1,j}|^2 + |x_{2,j}|^2$ .

#### IV. BACK-STEPPING RECURSIVE DECENTRALIZED FINITE-TIME CONTROL

In this section, based on the idea of backstepping, a recursive decentralized finite-time trajectory tracking controller is designed. First, the following intermediate variables are selected

$$\begin{cases} z_{1,i} = x_{1,i} \\ z_{2,i} = x_{2,i} - \alpha_{z,i} \end{cases} \quad (i = 1, 2, \dots, 5) \quad (31)$$

The designed virtual control variable is

$$\alpha_{z,i} = -K_{\alpha 1,i} x_{1,i} - K_{\alpha 2,i} \text{sig}(x_{1,i})^{\nu_\alpha} \quad (32)$$

where  $K_{\alpha 1} = K_{\alpha 2} = K_\alpha$ ,  $K_{\alpha 2,i} > 0$  ( $i = 1, 2, \dots, 5$ ), and  $0 < \nu_\alpha < 1$ , which is a nonlinear function.

$$\text{sig}(x_{1,i})^{\nu_\alpha} = \text{sgn}(x_{1,i}) |x_{1,i}|^{\nu_\alpha} \quad (33)$$

where  $\text{sgn}(\cdot)$  is a sign function.

The following lemmas are introduced before proceeding with the proof of stability.

**Lemma 1** [42] For the following system

$$\dot{\mathbf{x}} = \mathbf{f}(\mathbf{x}), \mathbf{f}(\mathbf{0}) = \mathbf{0}, \mathbf{x} \in \mathbb{R}^n \quad (34)$$

If there exists a positive definite continuous function  $V(\mathbf{x})$  defined on the origin neighborhood  $U_0$  and real numbers  $a > 0$ ,  $b > 0$ , and  $0 < p < 1$  that satisfies

$$\dot{V}(\mathbf{x}) \leq -aV^p(\mathbf{x}) - bV(\mathbf{x}), \mathbf{x} \in U_0$$

then the system is finite-time stable.

For the following Lyapunov function

$$V_\alpha = \frac{1}{2} \mathbf{x}_1^T \mathbf{x}_1 \geq 0$$

when the designed virtual control variable  $\alpha_{z,i}$  makes  $z_{2,i} \rightarrow 0$ , there is  $\dot{z}_{1,i} = \dot{x}_{1,i} = \alpha_{z,i}$ , and

$$\begin{aligned} \dot{V}_\alpha &= \mathbf{x}_1^T \dot{\mathbf{x}}_1 = \sum_{i=1}^5 x_{1,i} \alpha_{z,i} \\ &\leq -2K_{\alpha 1}^{\min} V_\alpha - 2^{\frac{\nu_\alpha+1}{2}} K_{\alpha 2,i}^{\min} (V_\alpha)^{\frac{\nu_\alpha+1}{2}} \end{aligned}$$

where  $K_{\alpha 1}^{\min}$  and  $K_{\alpha 2}^{\min}$  are the minimum of  $K_{\alpha 1,i}$  and  $K_{\alpha 2,i}$  ( $i = 1, 2, \dots, 5$ ), respectively. Hence, according to Lemma 1, state  $\mathbf{x}_1$  can converge to an equilibrium in a finite time.

Next, we analyze the relationship between the system disturbance boundary (30) and the intermediate variables (31). For  $\alpha_{z,i}$ , according to Eq. (33), there is

$$\begin{aligned} |\alpha_{z,i}| &= |K_{\alpha 1,i} x_{1,i} + K_{\alpha 2,i} \text{sig}(x_{1,i})^{\nu_\alpha}| \\ &= |K_{\alpha 1,i} \text{sgn}(x_{1,i})| |x_{1,i}| + K_{\alpha 2,i} \text{sgn}(x_{1,i}) |x_{1,i}|^{\nu_\alpha} \\ &= |\text{sgn}(x_{1,i})(K_{\alpha 1,i} |x_{1,i}| + K_{\alpha 2,i} |x_{1,i}|^{\nu_\alpha})| \\ &= |(K_{\alpha 1,i} |x_{1,i}| + K_{\alpha 2,i} |x_{1,i}|^{\nu_\alpha})| \\ &\geq K_{\alpha 1,i} |x_{1,i}| \end{aligned}$$

Then, according to the definition of  $z_{2,i}$ , there is

$$|\alpha_{z,i}| = |z_{2,i} - x_{2,i}| \leq |z_{2,i}| + |x_{2,i}|$$

Thus, there is

$$K_{\alpha 1,i} |x_{1,i}| \leq |z_{2,i}| + |x_{2,i}| \quad (35)$$

For Eq. (28), there is a  $p_1, p_2 \geq 0$  that makes  $\|\mathbf{q}_{\theta i}\| \leq p_1 \|\theta_i\| + p_2$  [26], then

$$|x_{2,i}| \leq p_1 |x_{1,i}| + p_2 \quad (36)$$

where  $p_d = p_1 |\theta_{d,\theta i}| + |q_{d,\theta i}| + p_2 \geq 0$ , which is bounded. From Equations (33) and (34),

$$K_{\alpha 1,i} |x_{1,i}| \leq |z_{2,i}| + |x_{2,i}| \leq |z_{2,i}| + p_1 |x_{1,i}| + p_d$$

That is

$$(K_{\alpha 1,i} - p_1) |x_{1,i}| \leq |z_{2,i}| + p_d$$

There are  $p_1$  and  $p_d$ , where  $p_1 < K_{\alpha 1,i}$ , that makes the state variable bounded

$$|x_{1,i}| \leq \frac{1}{(K_{\alpha 1,i} - p_1)} |z_{2,i}| + \frac{p_d}{(K_{\alpha 1,i} - p_1)} \quad (37)$$

Substituting Eq. (37) into Eq. (36), another state variable boundary is

$$|x_{2,i}| \leq \frac{p_1}{K_{\alpha 1,i} - p_1} |z_{2,i}| + \frac{K_{\alpha 1,i} p_d}{K_{\alpha 1,i} - p_1} \quad (38)$$

Therefore, according to Eq. (36) based on the backstepping intermediate variable  $z_{2,i}$ , the disturbance boundary (30) in the recursive decentralized control model is written as

$$I_{q0,\theta i}^{-1} |d_{\theta,\theta i}^{\text{rd}} + d_{x,\theta i}| \leq \delta_{Zi} \sum_{j=1}^5 Z_j \quad (39)$$

where  $\delta_{Zi} \geq 0$  and  $Z_j = 1 + |z_{2,i}| + |z_{2,i}|^2$  [26].

Based on the virtual control variable (32), the following control law is designed for model (28),

$$\begin{aligned} u_{\theta i} = I_{q0,\theta i} (\dot{q}_{d,\theta i} + \dot{\alpha}_{z,i} - x_{1,i} - K_{z1,i} \text{sig}(z_{2,i})^{\nu_\alpha} \\ - K_{z2,i} \text{sgn}(z_{2,i})) + F_{Tx,\theta i} + \dot{q}_{d,\theta i}^{\text{rd}} \end{aligned} \quad (40)$$

where  $K_{z1,i} > 0$  and  $K_{z2,i} > 0$  ( $i = 1, \dots, 5$ ) are the control parameters. The feedback linearization compensation term  $\dot{q}_{d,\theta i}^{\text{rd}}$  is calculated recursively from the root body to the end body, and  $F_{Tx,\theta i}$  is calculated recursively from the end body to the root body.

**Lemma 2** [43] For the system in Eq. (34), if there exists a positive definite continuous function  $V(\mathbf{x})$  defined on the origin neighborhood  $U_0$  and real numbers  $a > 0, b > 0$ , and  $0 < p < 1$  that satisfies

$$\dot{V}(\mathbf{x}) \leq -a V^p(\mathbf{x}), \mathbf{x} \in U_0$$

the system (34) is finite-time stable, that is, the system can converge to an equilibrium in a finite time.

For the Lyapunov function,

$$V_d = \frac{1}{2} \sum_{i=1}^5 x_{1,i}^2 + \frac{1}{2} \sum_{i=1}^5 z_{2,i}^2 \geq 0$$

Take the derivative with respect to time, and substitute it into the control law (40),

$$\begin{aligned} \dot{V}_d &= \sum_{i=1}^5 x_{1,i} \dot{x}_{1,i} + \sum_{i=1}^5 z_{2,i} \dot{z}_{2,i} \\ &= \sum_{i=1}^5 x_{1,i} \alpha_{z,i} - \sum_{i=1}^5 z_{2,i} (K_{z1,i} \text{sig}(z_{2,i})^{\nu_\alpha} + K_{z2,i} \text{sgn}(z_{2,i})) \\ &\quad + \sum_{i=1}^5 z_{2,i} I_{q0,\theta i}^{-1} (d_{\theta,\theta i}^{\text{rd}} + d_{x,\theta i}) \\ &= \sum_{i=1}^5 x_{1,i} \alpha_{z,i} - \sum_{i=1}^5 K_{z1,i} z_{2,i} \text{sig}(z_{2,i})^{\nu_\alpha} - \sum_{i=1}^5 K_{z2,i} |z_{2,i}| \\ &\quad + \sum_{i=1}^5 z_{2,i} I_{q0,\theta i}^{-1} (d_{\theta,\theta i}^{\text{rd}} + d_{x,\theta i}) \\ &\leq \sum_{i=1}^5 x_{1,i} \alpha_{z,i} - \sum_{i=1}^5 K_{z1,i} z_{2,i} \text{sig}(z_{2,i})^{\nu_\alpha} - \sum_{i=1}^5 K_{z2,i} |z_{2,i}| \\ &\quad + \sum_{i=1}^5 \delta_{Zi} |z_{2,i}| \sum_{j=1}^5 Z_j \end{aligned}$$

where Eq. (39) is utilized in the last step above.

According to Chebyshev's inequality, because  $|z_{2,i}| \leq |z_{2,j}| \Leftrightarrow Z_i \leq Z_j$ , there is

$$\sum_{i=1}^5 |z_{2,i}| \delta_{Zi} \sum_{j=1}^5 Z_j \leq 5 \sum_{i=1}^5 \delta_{Zi} |z_{2,i}| Z_i \quad (41)$$

Substitute the above equation into  $\dot{V}_d$ , then

$$\begin{aligned} \dot{V}_d &\leq \sum_{i=1}^5 x_{1,i} \alpha_{z,i} - \sum_{i=1}^5 K_{z1,i} z_{2,i} \text{sig}(z_{2,i})^{\nu_\alpha} \\ &\quad - \sum_{i=1}^5 |z_{2,i}| (K_{z2,i} - 5 \delta_{Zi} Z_i) \end{aligned} \quad (42)$$

Therefore, there exists  $K_{z2,i} \geq 5 \delta_{Zi} Z_i$  that makes

$$\dot{V}_d \leq \sum_{i=1}^5 x_{1,i} \alpha_{z,i} - \sum_{i=1}^5 K_{z1,i} z_{2,i} \text{sig}(z_{2,i})^{\nu_\alpha}$$

Substitute the virtual control variable (32) into the above equation, then

$$\dot{V}_d \leq -2^{\frac{\nu_\alpha+1}{2}} K_{\alpha z}^{\min} (V_d)^{\frac{\nu_\alpha+1}{2}}$$

where  $K_{\alpha z}^{\min}$  is the minimum of  $K_{\alpha 2}^{\min}$  and  $K_{z1}^{\min}$ , and  $K_{z1}^{\min}$  is the minimum of  $K_{z1,i}$  ( $i = 1, 2, \dots, 5$ ).

When  $x_{1,i}=0$  and  $\dot{x}_{1,i} \neq 0$ , the derivative of the nonlinear function  $(\text{sig}(x_{1,i})^{\nu_\alpha})' = \nu_\alpha |x_{1,i}|^{\nu_\alpha-1} \dot{x}_{1,i}$  is infinite, which will lead to the singularity of the control law. Therefore, a threshold is set in the neighborhood of  $x_{1,i}=0$  ( $i = 1, 2, \dots, 5$ ) to improve the singularity. The following function is defined

$$f_{ds}(x_{1,i}) = \begin{cases} |x_{1,i}| & |x_{1,i}| \geq \lambda_{\text{sig}} \\ |\Delta_{\text{sig}}| & |x_{1,i}| < \lambda_{\text{sig}} \end{cases} \quad (43)$$

where,  $\lambda_{\text{sig}}$  and  $\Delta_{\text{sig}}$  are small positive constants [44]. According to Lemma 2, the control laws (32) and (40) can ensure that

the system (28) converge to the neighborhood  $|x_{1,i}| < \lambda_{\text{sig}}$  near the equilibrium point in a finite time.

## V. NUMERICAL RESULTS

The recursive decentralized back-stepping finite-time controller (RFT) is applied to the trajectory tracking control of the SPRBM. The trajectory tracking control task is capturing a cylindrical target in front of SPRBM. As shown in Fig. 6, by choosing four states, the motion of SPRBM is divided into three stages when capturing the target. The first stage is to expand the capture net port to the maximum unfolding state, the second is to lower the unfolded capture net port, and the third is to achieve a three-point clamping capture configuration. At this time, the target is captured. However, since the collision the target needs to be considered in the third stage, while the trajectory tracking controller proposed in this work cannot solve this problem, only the trajectory tracking control task in the first stage is involved in the simulations. In the numerical example, at the initial moment, the center of the SPRBM is  $[0, 0, 0]^T$  m, the attitude in Euler angle is  $[0, 0.2618, 0]^T$  rad, and each joint is in flexion. From 0–10s is the first stage. At this stage, the attitude changes to  $[0, 0, 0]^T$  rad according to the predetermined trajectory, and the rotation angle  $\theta_1$  changes to  $-0.2618$  rad, whereas the other joints move to the maximum extension state 1. This stage is also called the tracking stage. The next 10s are called the stable stage, in which each joint maintains the above state, with the angular velocity and angular acceleration of zero. Then, the 4–3–·–3–4 polynomial planning method is used to plan the trajectories of the independent joints, and the desired trajectories of the independent joints are shown in Fig. 7.

To verify the robustness of the controller, the mass parameters of the controller were taken as 5/6ths of the actual values listed in Table I, and these values were then used to calculate the nominal mass matrix  $M_{\theta 10}$  and the nonlinear term  $F_{t,\theta 1}$  to simulate the mass uncertainty of the system. In addition, a  $5 \times 10^{-3} \sin(\pi t)$  N disturbance force was exerted on the three translational degrees of freedom of the SPRBM, and a  $0.001 \sin(2\pi t)$  Nm disturbance moment was applied on the three rotational degrees of freedom. The controller gains were  $K_{\alpha 1,i} = K_{\alpha 2,i} = 15$  and  $\nu_\alpha = 0.8$ , and the values of  $K_{z1,i}$  and  $K_{z2,i}$  were consistent with the corresponding elements of  $K_{z1}$  and  $K_{z2}$  in Eq. (47).

To achieve the position and attitude tracking and control of the main bus of the SPRBM, the error model is established as follows:

$$\begin{cases} \dot{x}_1 = T_b x_2 \\ \dot{x}_2 = M_b^{-1} (F_{tb} + u_b + d_b) \end{cases} \quad (44)$$

where  $x_1 = [R_e \Psi_e]$ ,  $\Psi_e = \frac{1}{2\sqrt{1+\text{tr}(A_{d,b})}} (A_{d,b} - A_{d,b}^T)^\vee$  is the attitude error parameter [45], and  $\text{tr}(A_{d,b})$  is the trace of the matrix  $A_{d,b}$ . Symbol  $\vee$  denotes the original matrix of the antisymmetric cross-product matrix, and  $A_{d,b} = A_{e,d}^T A_{e,b}, A_{e,d}$  is the desired attitude matrix.  $x_2 = [v_e \omega_e]$ , where  $\omega_e = \omega_b - A_{b,e} \Omega_d$ ,  $\Omega_d$  is the

tracking angular velocity.  $T_b = \begin{bmatrix} A_{e,b} & \\ & T_\Psi \end{bmatrix}$ , and  $T_\Psi = \frac{1}{2\sqrt{1+\text{tr}(A_{d,b})}} [\text{tr}(A_{d,b}^T) U_{3 \times 3} - A_{d,b}^T + 2\Psi_e \Psi_e^T]$ . The nonlinear term is  $F_{tb} = \begin{bmatrix} -m_{b0} (A_{b,e} \dot{V}_d + \omega_b^\times v_b - \omega_b^\times A_{b,e} V_d) \\ -\omega_b^\times J_{b0} \omega_b - J_{b0} \omega_b^\times \omega_e - J_{b0} A_{d,b}^T \dot{\omega}_d \end{bmatrix}$ , and  $M_b = \begin{bmatrix} m_{b0} U_{3 \times 3} & \\ & J_{b0} \end{bmatrix}$ , where  $m_{b0}$  and  $J_{b0}$  are the nominal mass and nominal moment of inertia of the SPRBM, respectively,  $d_b$  is the disturbance term, and  $u_b$  is the control input. The finite-time position and attitude tracking control law are designed as

$$\begin{cases} u_b = -F_{tb} - K_{b1} \text{sgn}(s) - K_{b2} s \\ \quad - \gamma_b \beta_b M_b f_{ds}(x_1)^{\gamma_b-1} T_b x_2 \\ s = x_2 + \beta_b \text{sig}(x_1)^{\gamma_b} \end{cases} \quad (45)$$

where  $K_{b1} = 1 \times 10^{-4} \text{diag}(1, 1, 1, 1, 1, 1)$ ,  $K_{b2} = \text{diag}(20, 20, 20, 30, 30, 30)$ ,  $\beta_b = \text{diag}(10, 10, 10, 10, 10, 10)$ ,  $\gamma_b = 0.8$ ,  $\Delta_{\text{sig}} = 0.001$ , and  $\lambda_{\text{sig}} = 0.001$ .

The following three controllers are used for the same task to demonstrate their control characteristics.

The first controller is the backstepping centralized finite-time controller (CFT). The state space of the dynamic equation of the trajectory tracking error is as follows:

$$\begin{cases} \dot{x}_1 = x_2 \\ \dot{x}_2 = M_{\theta 10}^{-1} (u_{\theta 1} + d_{\theta 1} - F_{t,\theta 1}) - \dot{q}_{d,\theta 1} \end{cases} \quad (46)$$

The control law is

$$u_{\theta 1} = M_{\theta 10} (\dot{q}_{d,\theta 1} + \dot{\alpha}_z - x_1 - K_{z1} \text{sig}(z_2)^{\nu_\alpha} - K_{z2} \text{sgn}(z_2)) + F_{t,\theta 1} \quad (47)$$

where  $\dot{\alpha}_z = -\nu_\alpha K_\alpha f_{ds}(x_1)^{\nu_\alpha-1} \dot{x}_1$ ,  $z_2 = x_2 + K_\alpha \text{sig}(x_1)^{\nu_z}$ ,  $K_{z1} = \text{diag}(1.2, 1, 1, 1, 1)$ ,  $K_{z2} = 1 \times 10^{-4} \text{diag}(1, 1, 1, 1, 1)$ ,  $K_\alpha = \text{diag}(15, 15, 15, 15, 15)$ ,  $\nu_\alpha = 0.8$ ,  $\Delta_{\text{sig}} = 0.001$ , and  $\lambda_{\text{sig}} = 0.001$ .

The second controller is the backstepping decentralized finite-time controller (DFT). The state space of the dynamic equation of the trajectory tracking error is as follows:

$$\begin{cases} \dot{x}_{1,i} = x_{2,i} \\ \dot{x}_{2,i} = M_{\theta 10,ii}^{-1} (u_{\theta 1,i}^* + d_{\theta 1,i}^* - F_{t,\theta 1,i}^*) - \dot{q}_{d,\theta 1i} \end{cases} \quad (i = 1, \dots, 5) \quad (48)$$

The control law is

$$u_{\theta 1,i}^* = M_{\theta 10,ii} (\dot{q}_{d,\theta 1i} + \dot{\alpha}_{z,i}^* - x_{1,i} - K_{z1,i}^* \text{sig}(z_{2,i}^*)^{\nu_\alpha^*} - K_{z2,i} \text{sgn}(z_{2,i}^*)) + F_{t,\theta 1i}^* \quad (49)$$

where  $\dot{\alpha}_{z,i}^* = -\nu_\alpha^* K_{\alpha,i}^* f_{ds}(x_{1,i})^{\nu_\alpha^*-1} \dot{x}_{1,i}$ ,  $z_{2,i}^* = x_{2,i} + K_{\alpha,i}^* \text{sig}(x_{1,i})^{\nu_\alpha^*}$ , the values of  $K_{z1,i}^*$ ,  $K_{z2,i}$  and  $K_{\alpha,i}^*$  are consistent with the corresponding elements in  $K_{z1}$ ,  $K_{z2}$  and  $K_\alpha$  in Eq. (47), and the values of  $\nu_\alpha^* = \nu_\alpha = 0.8$ ,  $\Delta_{\text{sig}}$  and  $\lambda_{\text{sig}}$  are also the same as in Eq. (47).

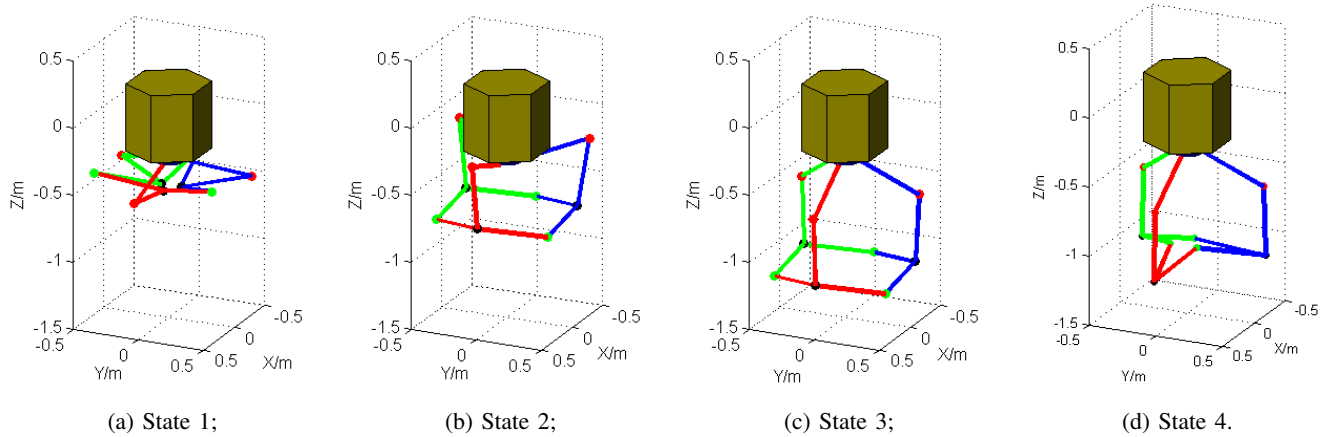


Fig. 6: Schematic diagram of the system configuration in the selected states (a) State 1: flexion; (b) State 2: maximum extension state 1; (c) State 3: maximum extension state 2; (d) State 4: three-point clamping state [19].

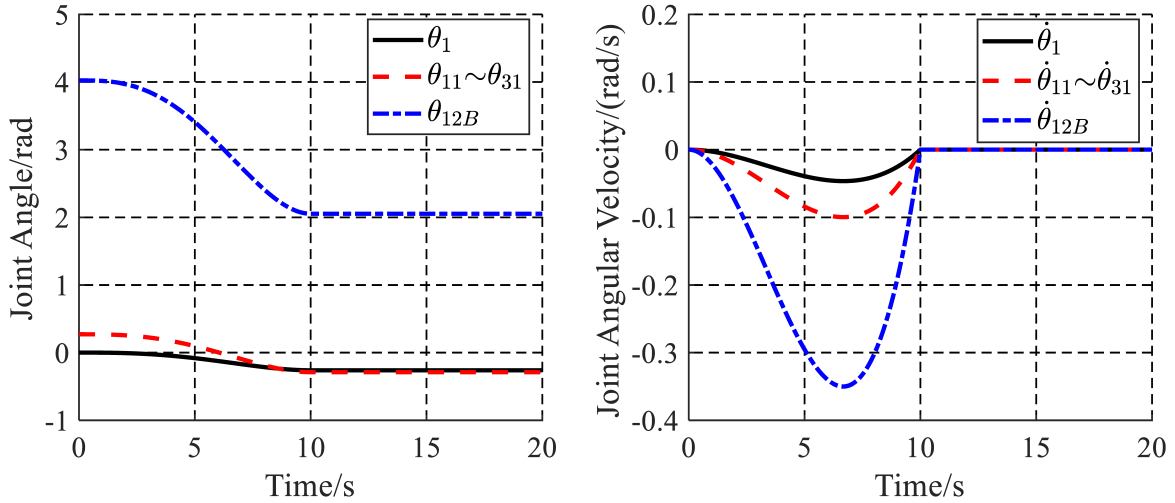


Fig. 7: Desired trajectory of each joint.

TABLE II: Joint states [19]

States	Flexion state	Maximum extension state 1	Maximum extension state 2	Three-point clamping state
Independent joints	$\theta_1$ (rad)	0	0	0
	$\theta_{11}, \theta_{21}, \theta_{31}$ (rad)	0.2713	-0.2894	0.5721
	$\theta_{12B}$ (rad)	4.0226	2.0534	0.4027
Dependent joints	$\theta_{12}, \theta_{22}, \theta_{32}$ (rad)	5.8795	5.1731	4.1101
	$Q_{12A}, Q_{22A}, Q_{32A}$ (rad)	[0.2275, 0.4912, 0.6695, 0.5086] <sup>T</sup>	[0.7067, 0.6173, 0.0245, 0.3448] <sup>T</sup>	[0.4885, 0.5986, 0.0663, 0.3077] <sup>T</sup>

The third controller is the recursive decentralized PD controller (RPD)

$$u_{\theta i}^{rd} = F_{Tx,\theta i} - K_{Pi}x_{1,i} - K_{Di}x_{2,i} + \dot{q}_{d,\theta i} \quad (50)$$

where the values of  $K_{Pi}$  and  $K_{Di}$  are consistent with the corresponding elements in  $\mathbf{K}_P$  and  $\mathbf{K}_D$ , and  $\mathbf{K}_P = [30, 10, 10, 10, 30]$ ,  $\mathbf{K}_D = [20, 6, 6, 6, 15]$ .

The control torque in the independent joint space is shown in Figs. 8-11. In the tracking stage, the curves of the control torque of the DFT, RPD and RFT were close. The order of magnitude of the output control torque was CFT>RFT≈RPD>DFT. This was because the DFT did not consider the disturbance caused by other joints in the control, and the RFT and RPD only partially considered the distur-

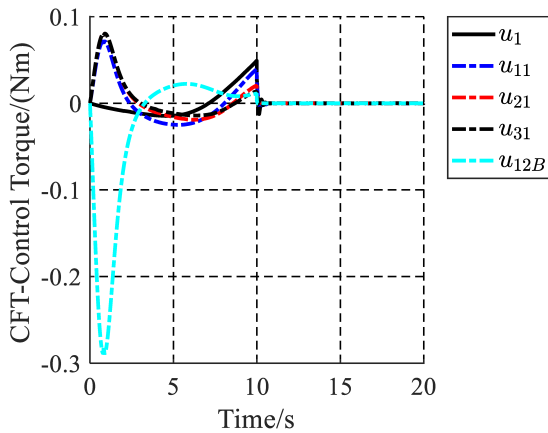


Fig. 8: Control torque output in the independent joint space using the CFT.

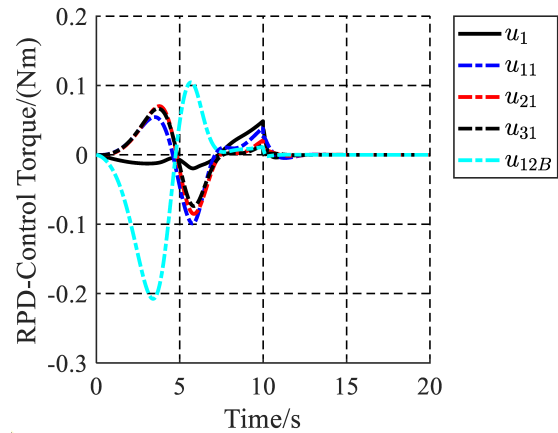


Fig. 10: Control torque output in the independent joint space using the RPD.

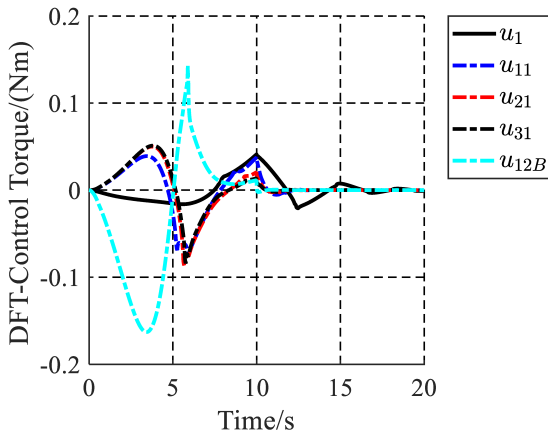


Fig. 9: Control torque output in the independent joint space using the DFT.

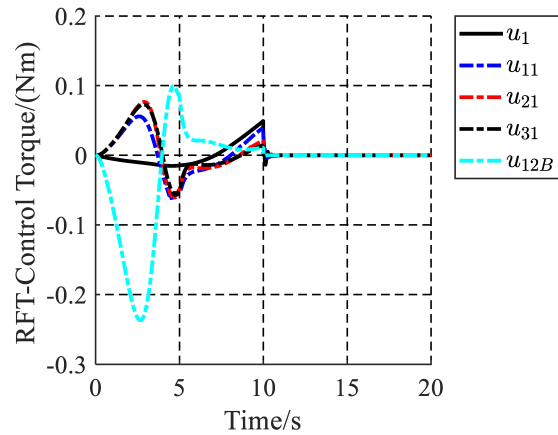


Fig. 11: Control torque output in the independent joint space using the RFT.

bance of other joints, whereas the CFT considered the state of the whole system. In the stable stage, the control torques of the CFT, RFT, and RPD were close to zero, while the control torque of the DFT was still large.

Figs.12-15 and Table. III present the tracking errors of the joint angle and angular velocity of the controllers. CFT has the highest control accuracy and convergence rate, and the DFT has the lowest accuracy and convergence rate, while the RFT and RPD are in the middle. To compare the real-time performance of each controller, Table. IV shows the calculation time of the whole simulation process of each controller in the same simulation environment. Under the same simulation environment, the CFT has the longest calculation time, the DFT has the shortest calculation time, and the RFT and RPD are in the middle. Comparing the simulation results of the two recursive decentralized controllers, the RFT has a slightly higher control accuracy and significantly higher convergence rate than the RPD, whereas the calculation time of the RFT is slightly longer than the RPD. Overall, the RFT is superior to the RPD.

In addition, in order to show the impact of the multiplicity

of initial conditions on the performance metrics, 300 groups of Monte Carlo simulations are developed. In the simulations, the ratio of the mass parameters of the controller to the actual values listed in Table. 1, sign as 'diss-rate', is selected as a uniformly distributed random value. The distribution of diss-rate is shown in Fig. 16. The other parameters and settings are the same as in previous experiments. The Monte Carlo simulation results are shown in Fig. 17. The results indicate that different values of diss-rate have no significant impact on control performances.

## VI. CONCLUSION

In the present study, we proposed a backstepping recursive decentralized finite-time controller for trajectory tracking control of a SPRBM. The controller regarded the SPRBM as a series of interrelated subsystems, and the interaction between the subsystems was modeled by the recursive algorithm. Then, the nonlinear torque term and the desired generalized acceleration coupling term were compensated. The compensated error model was controlled by a finite-time control law. Compared with the centralized control scheme, the proposed

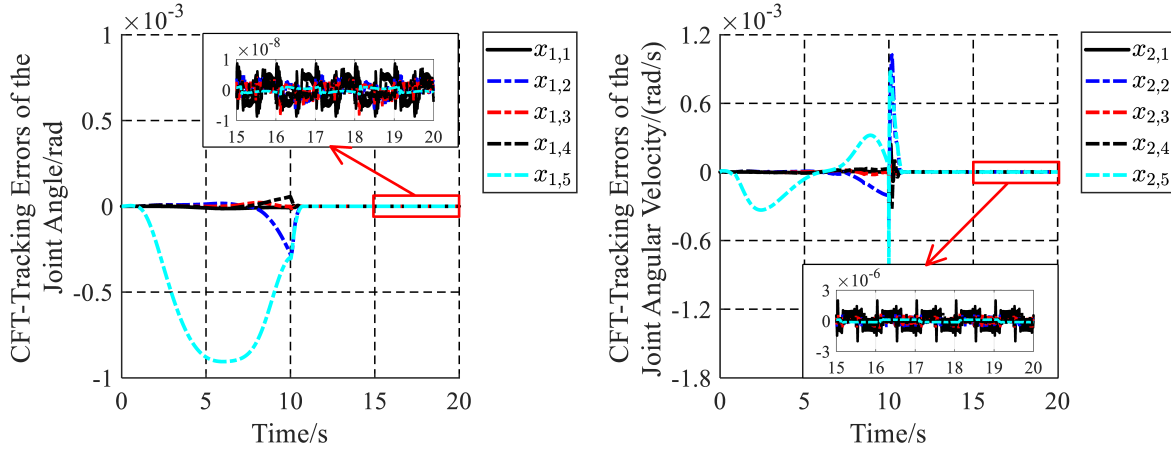


Fig. 12: Tracking errors of the joint angle and angular velocity using the CFT.

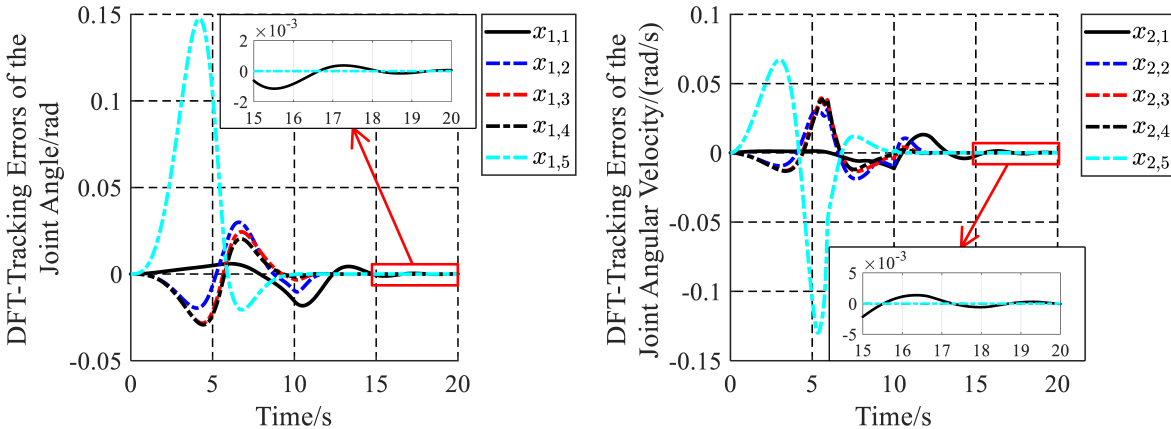


Fig. 13: Tracking errors of the joint angle and angular velocity using the DFT.

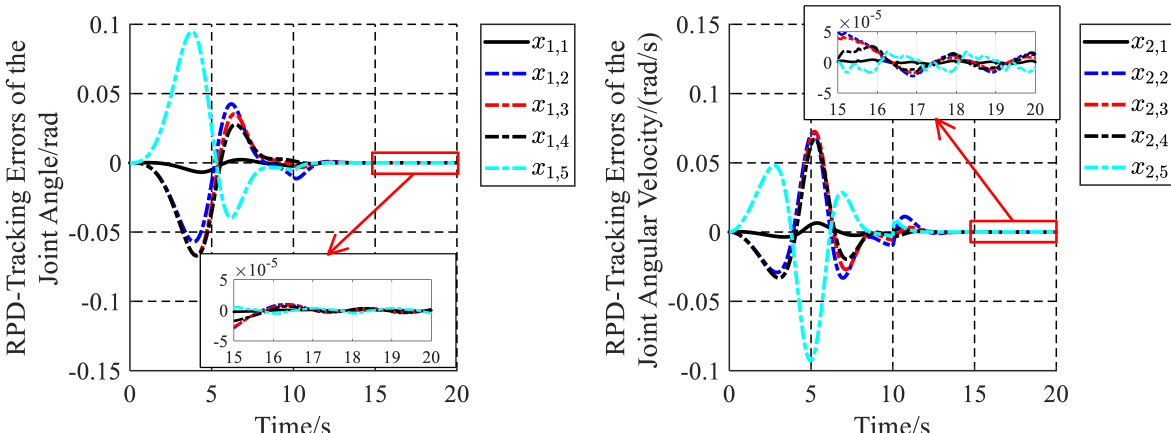


Fig. 14: Tracking errors of the joint angle and angular velocity using the RPD.

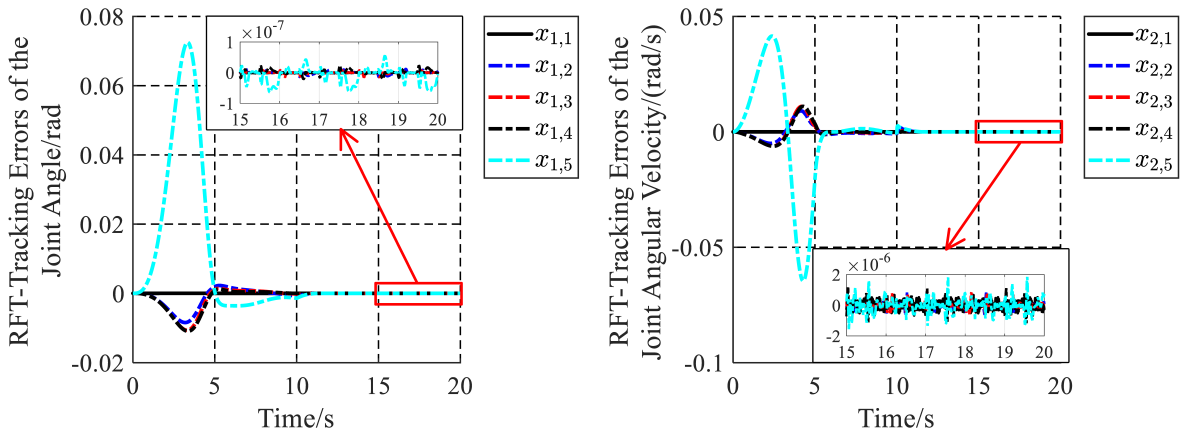


Fig. 15: Tracking errors of the joint angle and angular velocity using the RFT.

TABLE III: Order of magnitude of the dynamic error of each controller

Controller	Maximum dynamic error in the tracking stage		Maximum dynamic error in the stable stage	
	Error of the joint angle (rad)	Error of the joint angular velocity (rad/s)	Error of the joint angle (rad)	Error of the joint angular velocity (rad/s)
CFT	$9.06 \times 10^{-4}$	$1.02 \times 10^{-3}$	$8.68 \times 10^{-9}$	$1.99 \times 10^{-6}$
DFT	$1.47 \times 10^{-1}$	$1.30 \times 10^{-1}$	$1.14 \times 10^{-3}$	$2.04 \times 10^{-3}$
RPD	$9.46 \times 10^{-2}$	$9.25 \times 10^{-2}$	$2.90 \times 10^{-5}$	$5.00 \times 10^{-5}$
RFT	$7.23 \times 10^{-2}$	$6.37 \times 10^{-2}$	$6.38 \times 10^{-8}$	$1.85 \times 10^{-6}$

TABLE IV: Calculation time of the whole process of different controllers

Controller	Calculation time (s)
CFT	6.44
DFT	0.54
RPD	2.89
RFT	3.20

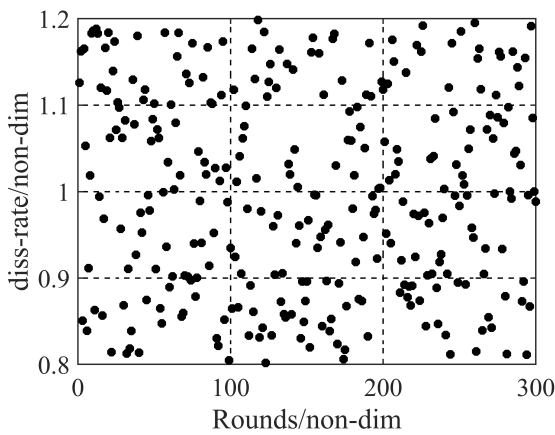


Fig. 16: The distribution of diss-rate.

control scheme does not require an accurate dynamic model and has less computation time. Moreover, since it considered the interaction between the various subsystems, the control performance was superior to that of the decentralized control

scheme.

Then, the numerical simulation of trajectory tracking control using the SPRBM mechanism was carried out. The results were compared with that of the backstepping centralized finite-time control scheme, the backstepping decentralized finite-time control scheme, and the recursive decentralized PD control scheme. The simulation results showed that the centralized control scheme had the highest accuracy and convergence rate, and the longest calculation time. The decentralized control scheme had the lowest accuracy, the lowest convergence rate, and the shortest calculation time. The performance of the recursive decentralized control schemes was in the middle. Therefore, compared with centralized control strategies and decentralized control schemes, it can be seen from both the theory and simulation results that the proposed recursive decentralized control strategy based on the idea of backstepping and finite-time controller has compromised advantages in computation cost and control accuracy. Furthermore, compared with the recursive decentralized PD control scheme, the backstepping recursive decentralized finite-time control scheme proposed in this study had a higher control accuracy and convergence rate, i.e., superior tracking control performance.

It's undeniable that the proposed method is not perfect and still has certain limitations, especially for engineering applications. First, compliant control needs to be considered as there are contact collisions when capturing a target using SPRBM. Second, due to the uncertainty of the impact point, how to estimate the impact force through the installed sensors is also a problem worthy to be solved. Finally, the ability of SPRBM to capture rotating targets requires further analysis.

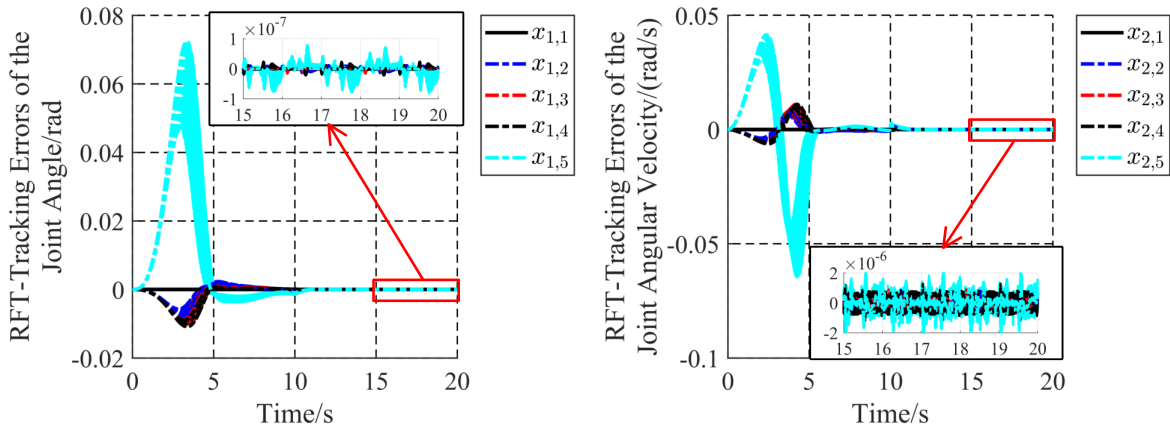


Fig. 17: Tracking errors of the joint angle and angular velocity using the RFT of the Monte Carlo simulations.

Since rotating targets have large kinetic energy, a large contact collision force may be generated when a target collides with the links of SPRBM during the capture process. What's worse, if the contact collision force exceeds the bearing range of the links, SPRBM may be damaged.

## APPENDIX A SPATIAL VECTOR ALGEBRA

The system dynamic and kinematic equations in this study are established based on space vector theory [45]. The definitions of some related variables and matrices are given for a rigid multibody system.

For the coordinate transformation matrix  $\mathbf{A}_{j,o(j)}$ , the corresponding extended coordinate transformation matrix  $\bar{\mathbf{A}}_{j,o(j)}$  is defined as

$$\bar{\mathbf{A}}_{j,o(j)} = \begin{bmatrix} \mathbf{A}_{j,o(j)} & \mathbf{0}_{3 \times 3} \\ \mathbf{0}_{3 \times 3} & \mathbf{A}_{j,o(j)} \end{bmatrix} \quad (51)$$

where  $\mathbf{0}_{3 \times 3}$  is a  $3 \times 3$  zero matrix. For a certain position vector  $\mathbf{p} = [p_x \ p_y \ p_z]^T$ , the corresponding position transformation matrix is defined as

$$\tilde{\mathbf{p}} = \begin{bmatrix} \mathbf{U}_{3 \times 3} & \mathbf{p}^{\times} \\ \mathbf{0}_{3 \times 3} & \mathbf{U}_{3 \times 3} \end{bmatrix} \quad (52)$$

where  $\mathbf{U}_{3 \times 3}$  is the  $3 \times 3$  identity matrix, and  $\mathbf{p}^{\times}$  is the antisymmetric cross product matrix of the vector  $\mathbf{p}$ .

$$\mathbf{p}^{\times} = \begin{bmatrix} 0 & -p_z & p_y \\ p_z & 0 & -p_x \\ -p_y & p_x & 0 \end{bmatrix} \quad (53)$$

The position transformation matrix is able to convert the addition and subtraction of the position vector into matrix multiplication. For example, Eq. (6) can be written as

$$\tilde{\mathbf{r}}_{j,o(j)} \tilde{\mathbf{r}}_{C_j,o(j)} = \tilde{\mathbf{r}}_{C_j} \quad (54)$$

For a rigid body  $j$  with a mass  $m_j$ , the moment of inertia relative to the center of mass  $C_j$  is  $\mathbf{J}_{C_j}$ , then the mass matrix

relative to the center of mass is defined as

$$\mathbf{I}_{C_j} = \begin{bmatrix} \mathbf{J}_{C_j} & \mathbf{0}_{3 \times 3} \\ \mathbf{0}_{3 \times 3} & m_j \mathbf{U}_{3 \times 3} \end{bmatrix} \quad (55)$$

According to the parallel axis theorem, the mass matrix of rigid body  $j$  relative to point  $O_j$  is

$$\mathbf{I}_j = \begin{bmatrix} \mathbf{J}_j & \mathbf{S}_j^{\times} \\ -\mathbf{S}_j^{\times} & m_j \mathbf{U} \end{bmatrix} = \tilde{\mathbf{r}}_{C_j} \mathbf{I}_{C_j} \mathbf{r}_{C_j}^T \quad (56)$$

where  $\mathbf{S}_j$  is the static moment of rigid body  $j$  relative to point  $O_j$ .

The angular velocity and velocity of point  $O_j$  on the rigid body  $j$  are defined as  $\omega_j$  and  $\mathbf{v}_j$ , which are described in the coordinate frame  $F_j$ , then the corresponding twist is defined as  $\mathbf{V}_j = [\omega_j^T \ \mathbf{v}_j^T]^T$ . The force and torque of point  $O_j$  at joint  $h_j$  are defined as  $\mathbf{n}_j$  and  $\mathbf{f}_j$ , which are described in the coordinate frame  $F_j$ . Then, the wrench is defined as  $\mathbf{F}_j = [\mathbf{n}_j^T \ \mathbf{f}_j^T]^T$ . Similarly, the twist relative to the inertial frame at the center of mass  $C_j$  is defined as  $\mathbf{V}_{C_j}$ , and the equivalent wrench of  $F_j$  at point  $C_j$  is  $\mathbf{F}_{C_j}$ . Then,

$$\begin{cases} \mathbf{F}_j = \tilde{\mathbf{r}}_{C_j} \mathbf{F}_{C_j} \\ \mathbf{V}_{C_j} = \tilde{\mathbf{r}}_{C_j}^T \mathbf{V}_j \end{cases} \quad (57)$$

The generalized velocity of the relative motion allowed by the joint  $h_j$  is denoted as

$$\mathbf{q}_j = \begin{bmatrix} \mathbf{q}_j^{\omega} \\ \mathbf{q}_j^v \end{bmatrix} \in \mathbb{R}^{N_j \times 1} \quad (58)$$

where  $\mathbf{q}_j^{\omega}$  and  $\mathbf{q}_j^v$  are the generalized velocity corresponding to  $\theta_j$  and  $\mathbf{l}_j$ , respectively.

To describe the allowed and constrained motion of the joint  $h_j$ , the projection matrices  $\Gamma_{Tj} \in \mathbb{R}^{6 \times N_j}$  and  $\Gamma_{Sj} \in \mathbb{R}^{6 \times (6-N_j)}$  are defined, which satisfy the following orthogonal relationship,

$$\begin{cases} \Gamma_{Tj}^T \Gamma_{Tj} = \mathbf{U} \in \mathbb{R}^{N_j \times N_j} \\ \Gamma_{Sj}^T \Gamma_{Sj}^T = \mathbf{U} \in \mathbb{R}^{(6-N_j) \times (6-N_j)} \\ \Gamma_{Sj}^T \Gamma_{Tj} = \mathbf{0} \in \mathbb{R}^{(6-N_j) \times N_j} \\ \Gamma_{Tj}^T \Gamma_{Sj} = \mathbf{0} \in \mathbb{R}^{N_j \times (6-N_j)} \end{cases} \quad (59)$$

The direction described by the matrix  $\Gamma_{Tj}$  corresponds to the generalized velocity  $q_j$  and the generalized active force. There is no relative motion in the directions described by  $\Gamma_{Sj}$ , which corresponds to the internal constraint force and constraint torque of the system.

## REFERENCES

- [1] J.-C. Liou, "The Top 10 Questions for Active Debris Removal," in *European workshop on active debris removal*, no. June, 2010.
- [2] N. L. Johnson, "Debris Removal: An Opportunity for Cooperative Research?" in *Space Situational Awareness Conference*, no. October, 2007.
- [3] Z. Meng, P. Huang, and J. Guo, "Approach Modeling and Control of an Autonomous Maneuverable Space Net," *IEEE Transactions on Aerospace and Electronic Systems*, vol. 53, no. 6, pp. 2651–2661, 2017.
- [4] Y. Zhang, R. Feng, Y. Yu, J. Liu, and H. Baoyin, "Asteroid Capture Dynamics and Control Using a Large-Scale Flexible Net," *IEEE Transactions on Aerospace and Electronic Systems*, vol. 58, no. 5, pp. 4033–4043, 2022.
- [5] Y. Zhao, P. Huang, F. Zhang, and Z. Meng, "Contact Dynamics and Control for Tethered Space Net Robot," *IEEE Transactions on Aerospace and Electronic Systems*, vol. 55, no. 2, pp. 918–929, 2019.
- [6] Y. Zhao, F. Zhang, and P. Huang, "Dynamic Closing Point Determination for Space Debris Capturing via Tethered Space Net Robot," *IEEE Transactions on Aerospace and Electronic Systems*, vol. 58, no. 5, pp. 4251–4260, 2022.
- [7] D. A. Sizov and V. S. Aslanov, "Space debris removal with harpoon assistance: choice of parameters and optimization," *Journal of Guidance, Control, and Dynamics*, vol. 44, no. 4, pp. 767–778, 2021.
- [8] A. Flores-Abad, M. A. Garcia Teran, I. U. Ponce, and M. Nandayapa, "Compliant Force Sensor-Less Capture of an Object in Orbit," *IEEE Transactions on Aerospace and Electronic Systems*, vol. 57, no. 1, pp. 497–505, 2021.
- [9] S. Jia and J. Shan, "Velocity-Free Trajectory Tracking and Active Vibration Control of Flexible Space Manipulator," *IEEE Transactions on Aerospace and Electronic Systems*, vol. 58, no. 1, pp. 435–450, 2022.
- [10] L. Zong, J. Luo, and M. Wang, "Optimal Concurrent Control for Space Manipulators Rendezvous and Capturing Targets under Actuator Saturation," *IEEE Transactions on Aerospace and Electronic Systems*, vol. 56, no. 6, pp. 4841–4855, 2020.
- [11] K. Li, Y. Zhang, and Q. Hu, "Dynamic modelling and control of a Tendon-Actuated Lightweight Space Manipulator," *Aerospace Science and Technology*, vol. 84, pp. 1150–1163, 2019.
- [12] Y. Zang, Y. Zhang, J. Zhang, Z. Guo, Y. Chen, and S. Chen, "Multipoint Contact Dynamics and the Detumbling Strategy for a Fast-Tumbling Target," *IEEE Transactions on Aerospace and Electronic Systems*, vol. 56, no. 4, pp. 3113–3122, 2020.
- [13] A. Flores-abad, O. Ma, K. Pham, and S. Ulrich, "A review of space robotics technologies for on-orbit servicing," *Progress in Aerospace Sciences*, vol. 68, pp. 1–26, 2014.
- [14] Y. Yao, D. Zhang, Y. Li, and R. Li, "Design and Analysis of Polyhedral Net Space Capture Mechanism," *Journal of Nanjing University of Aeronautics and Astronautics*, vol. 51, no. 3, pp. 263–271, 2019.
- [15] W. Liu, X. Li, W. Wen, J. Zhao, Y. Yao, and R. Li, "Kinematics analysis of composite space capture systems based on 3RRS-Bricard," *Acta Aeronautica et Astronautica Sinica*, vol. 42, no. 1, p. 523922, 2021.
- [16] C. Tian, Y. Fang, and Q. J. Ge, "Design and analysis of a partially decoupled generalized parallel mechanism for 3T1R motion," *Mechanism and Machine Theory*, vol. 140, pp. 211–232, 2019.
- [17] G. Li and P. Xu, "Design and analysis of a deployable grasping mechanism for capturing non-cooperative space targets," *Aerospace Science and Technology*, vol. 106, p. 106230, 2020.
- [18] J. Sun, L. Shao, L. Fu, X. Han, and S. Li, "Kinematic analysis and optimal design of a novel parallel pointing mechanism," *Aerospace Science and Technology*, vol. 104, p. 105931, 2020.
- [19] F. Liu, C. Guo, Q. Hu, X. Li, W. Liu, W. Wen, L. Liu, and J. Zhao, "Nonlinear kinematics of space parallel robot with Bricard mechanism," *Acta Astronautica*, vol. 208, no. February, pp. 367–380, 2023.
- [20] A. Nayak, "Kinematic analysis of reconfigurable parallel manipulators," Ph.D. dissertation, École centrale de Nantes, 2018.
- [21] S. Jia and J. Shan, "Continuous integral sliding mode control for space manipulator with actuator uncertainties," *Aerospace Science and Technology*, vol. 106, p. 106192, 2020.
- [22] R. Jin, P. Rocco, X. Chen, and Y. Geng, "LPV-Based Offline Model Predictive Control for Free-Floating Space Robots," *IEEE Transactions on Aerospace and Electronic Systems*, vol. 57, no. 6, pp. 3896–3904, 2021.
- [23] L. Shi, H. Yao, M. Shan, Q. Gao, and X. Jin, "Robust control of a space robot based on an optimized adaptive variable structure control method," *Aerospace Science and Technology*, vol. 1, p. 107267, 2021.
- [24] Y. Fan and W. Jing, "Inertia-free appointed-time prescribed performance tracking control for space manipulator," *Aerospace Science and Technology*, vol. 117, p. 106896, 2021.
- [25] M. Liu, "Decentralized PD and Robust Nonlinear Control for Robot Manipulators," *Journal of Intelligent and Robotic Systems*, vol. 20, no. 2, pp. 319–332, 1997.
- [26] Y. Tang, M. Tomizuka, G. Guerrero, and G. Montemayor, "Decentralized robust control of mechanical systems," *IEEE Transactions on Automatic Control*, vol. 45, no. 4, pp. 771–776, 2000.
- [27] B. Dong, F. Zhou, K. Liu, and Y. Li, "Decentralized robust optimal control for modular robot manipulators via critic-identifier structure-based adaptive dynamic programming," *Neural Computing and Applications*, vol. 32, pp. 3441–3458, 2020.
- [28] B. Dong, T. An, F. Zhou, K. Liu, and Y. Li, "Decentralized robust zero-sum neuro-optimal control for modular robot manipulators in contact with uncertain environments: theory and experimental verification," *Nonlinear Dynamics*, vol. 97, pp. 503–524, 2019.
- [29] Q. Hu, Y. Jia, and S. Xu, "Recursive Dynamics Algorithm for Multibody Systems with Variable-speed Control Moment Gyroscopes," *Journal of Guidance, Control, and Dynamics*, vol. 36, no. 5, pp. 1388–1398, 2013.
- [30] Q. Hu, C. Guo, Y. Zhang, and J. Zhang, "Recursive decentralized control for robotic manipulators," *Aerospace Science and Technology*, vol. 76, pp. 374–385, 2018.
- [31] D. Shen, L. Tang, Q. Hu, C. Guo, X. Li, and J. Zhang, "Space manipulator trajectory tracking based on recursive decentralized finite-time control," *Aerospace Science and Technology*, vol. 102, p. 105870, 2020.
- [32] L. Su, Q. Hu, and L. Zhang, "Recursive Decentralized Control for Trajectory Tracking of Flexible Space Manipulators," *IEEE Access*, vol. 7, pp. 39192–39206, 2019.
- [33] H. Duan, Y. Sun, and Y. Shi, "Bionic Visual Control for Probe-and-Drogue Autonomous Aerial Refueling," *IEEE Transactions on Aerospace and Electronic Systems*, vol. 57, no. 2, pp. 848–865, 2021.
- [34] H. Zhuang, Q. Sun, Z. Chen, and X. Zeng, "Robust adaptive sliding mode attitude control for aircraft systems based on back-stepping method," *Aerospace Science and Technology*, vol. 118, p. 107069, 2021.
- [35] X. Zhang, Q. Zong, L. Dou, R. Zhang, B. Tian, and W. Liu, "Finite-Time Distributed Attitude Synchronization for Multiple Spacecraft With Angular Velocity and Input Constraints," *IEEE Transactions on Control Systems Technology*, pp. 1–13, 2021.
- [36] K. Zhang, Y. Liu, and J. Tan, "Semiglobal Finite-Time Stabilization of Saturated Spacecraft Rendezvous System by Dynamic Event-Triggered and Self-Triggered Control," *IEEE Transactions on Aerospace and Electronic Systems*, vol. 58, no. 6, pp. 5030–5042, 2022.
- [37] H. Gui and A. H. de Ruiter, "Global finite-time attitude consensus of leader-following spacecraft systems based on distributed observers," *Automatica*, vol. 91, pp. 225–232, 2018.
- [38] Z. Anjum and Y. Guo, "Finite Time Fractional-order Adaptive Back-stepping Fault Tolerant Control of Robotic Manipulator," *International Journal of Control, Automation and Systems*, vol. 19, pp. 301–310, 2021.
- [39] M. Siavash, V. J. Majd, and M. Tahmasebi, "A practical finite-time back-stepping sliding-mode formation controller design for stochastic nonlinear multi-agent systems with time-varying weighted topology," *International Journal of Systems Science*, vol. 51, no. 3, pp. 488–506, 2020.
- [40] P. A. Hosseiniabadi, A. S. S. Abadi, M. K. Khosravani, and M. Rahimi, "Free chattering and finite time in a high order system by terminal back-stepping and terminal sliding mode control techniques," in *2017 IEEE 4th International Conference on Knowledge-Based Engineering and Innovation, KBEI 2017*, 2017, pp. 0476–0480.
- [41] S. Lin and S. K. Singh, "Decentralized Adaptive Controller Design for Large-Scale Systems with Higher Order Interconnections," *IEEE Transactions on Automatic Control*, vol. 37, no. 8, pp. 1106–1118, 1991.
- [42] S. Yu, X. Yu, B. Shirinzadeh, and Z. Man, "Continuous finite-time control for robotic manipulators with terminal sliding mode," *Automatica*, vol. 41, no. 11, pp. 1957–1964, 2005.
- [43] S. P. Bhat and D. S. Bernstein, "Lyapunov analysis of finite-time differential equations," in *Proceedings of the American Control Conference*, vol. 3, 1995, pp. 1831–1832.

- [44] D. Zhao, S. Li, and Q. Zhu, "A new TSMC prototype robust nonlinear task space control of a 6 DOF parallel robotic manipulator," *International Journal of Control, Automation and Systems*, vol. 8, no. 6, pp. 1189–1197, 2010.
- [45] T. Lee, "Exponential stability of an attitude tracking control system on SO(3) for large-angle rotational maneuvers," *Systems and Control Letters*, vol. 61, pp. 231–237, 2012.



**Chuandong Guo** was born in Sichuan, China, in 1995. He received the B. S. and Ph.D. degrees in science in aeronautical and astronautical engineering from Beijing Institute of Technology, Beijing, China, in 2017 and 2023, respectively. He is currently serving as a lecturer at Sichuan University of Science and Engineering.

His research interests include attitude dynamics and control of complex flexible spacecraft and gyro control law design.



**Fei Liu** was born in Beijing, China, in 1992. She received the Ph.D. degrees in science in aeronautical and astronautical engineering from Beijing Institute of Technology, Beijing, China, in 2020. She is currently an engineer in Beijing Institute of Aerospace Systems Engineering.

Her research interests include GNC and mission design of spacecraft.



**Quan Hu** received his B.S. and Ph.D. degrees in aerospace engineering from Beihang University, Beijing, China, in 2009 and 2014, respectively. From 2014 to 2016, he was a postdoctoral fellow at the School of Aerospace Engineering, Beijing Institute of Technology, China. He joined the same institution as an Assistant Professor in 2016 and has been serving as an Associate Professor since 2021.

His research interests include attitude control and vibration suppression of flexible spacecraft, as well as the dynamics and control of space robots.